이학박사 학위논문

A study of the atomic force microscopy lithography and its applications

원자힘 현미경을 이용한 식각 및 그 응용에 대한 연구

2014년 2월

서울대학교 대학원

물리천문학부

전 승 희

A study of the atomic force microscopy lithography and its applications

원자힘 현미경을 이용한 식각 및
그 응용에 관한 연구

지도교수 제 원 호

이 논문을 이학박사학위 논문으로 제출함.
2013년 11월

서울대학교 대학원
물리천문학부
전 승 희

전승희의 이학박사 학위논문을 인준함.
2013년 12월

위 원 장 차 국 린 (인)

부위원장 제 원 호 (인)

위 원 김 정 구 (인)

위 원 홍 승 훈 (인)

위 원 안 희 준 (인)

A study of the atomic force microscopy lithography and its applications

SeungHee Jeon

Supervised by

Professor Wonho Jhe

A Dissertation

Submitted to the Faculty of

Seoul National University

In Partial Fulfillment of the Requirements

For the Degree of Doctor of Philosophy

February 2014

Department of Physics and Astronomy

Graduate School

Seoul National University

Abstract

We fabricated reproducible quantum dots and nanowires while minimizing atomic force microscopy (AFM) tip damage. Uniform patterns of quantum dots and nanowires were reproducibly fabricated by creating holes in a double-layer structure using AFM indentation, dry-etching of polymer resists, and metal deposition through the indentation holes. The double-layer was fabricated by depositing a thin gold layer onto a polymethyl methacrylate (PMMA) layer on a silicon dioxide substrate. The indentation force exerted on the double-layer was set so that the AFM tip penetrated the thin gold layer without the tip touching the silicon dioxide substrate in order to minimize of AFM tip. This double-layer indentation was used to create a pattern of holes in the thin gold layer which acts as a metal mask in the dry-etching process. The PMMA was exposed to an isotropic O_2 plasma etchant through the holes in the indentation pattern to form an undercut between the substrate and the gold layer. The undercut enables the deposition of metal on the substrate without having polymer residues. Quantum dots were subsequently created through the deposition of gold on the exposed silicon dioxide substrate through the indentation holes.

Gold nanowires were also fabricated by consecutive-hole-indentation method by adjusting the distance between the holes using the same double-layer indentation method. The topographic and electrical measurements of the fabricated gold nanowires suggest that our method is capable of making uniform and reproducible nanowires. The scanning electron microscopy images of the tips confirmed that the consecutive-hole-

indentation method is less invasive than the conventional ploughing method, where constant tip contact occurs with the substrate during the formation of nanowires. We also investigated removal of the bulge containing the metal by sonification.

We investigated the dependence of indented structures on the speed at which a tilted AFM tip penetrated a double-layer consisting of metal and an organic material for the potential development of a reproducible AFM-based nanolithography technique. Distorted half-circles were formed by the AFM tip when the indentation speed was slower than 5 μm/s for gold and PMMA thin film, whereas triangular structures were formed when the speed was faster than 5 μm/s. As the indentation speed increased, the depth of the indented structure also increased while its length decreased. We found that such structural changes from the tetrahedral shape of AFM tip originated from the rotational motion of the tilted AFM tip in the double-layer.

Keywords: AFM (atomic force microscopy), Double-layer, Consecutive-hole-indentation method, Indentation lithography, PMMA, Quantum dot, Nanowire, Indentation speed

Student ID: *2002-30936*

Contents

List of Figures

Chapter 1

Introduction

1.1 Nanolithography with atomic force microscopy

1.1.1 Overview

As the size of electronic devices gets smaller, many methods of fabrication of nano-electronic devices have been developed using nanolithography techniques such as electron-beam lithography (EBL)[1],[2],[3], x-ray lithography[4],[5], focused ion beam lithography[6], nanoimprint lithography[7],[8], and atomic force microscopy (AFM) nanolithography. EBL as a method of the maskless direct lithography is the method which uses a focused beam of electron. The resist is exposed to the focused electron, and then the solubility of resist is changed. Using this property, it can be selectively removed either the exposed area or unexposed area of the resist. EBL has high resolution with sub-10 nm, but has drawbacks like low throughput. X-ray lithography can be overcome optical limitation because of extremely short wavelength of 1 nm. But it also has drawbacks like as difficulty of mask fabrication. Nanoimprint lithography is a simple nanolithography method changing the shape of the sample using mechanical deformation of polymer with high resolution, low cost and high throughput. But, this method has economical drawback because the unit price of the mold which is used in nanoimprint lithography, is very expensive.

Among these techniques, nanolithography using AFM is a more versatile method when compared to the electron-beam lithography or focused ion beam lithography. AFM can perform the simultaneously measurement and lithography on the sample (in-situ fabrication). It performs inexpensively in a comparatively simple process, and it is able to fabricate nanostructures without risk of sample damage. This method also has advantages in making such nanoscale devices through easy fabrication of nanostructures to desired locations and sizes. However, it has disadvantages, such as poor reproducibility due to tip damage and low throughput due to the low speed of AFM system and difficulty of application over a large area. Yet, this method is able to reproduce nanostructures at specified locations, which makes it useful when applied to nanosystems because it can easily make various patterns.

1.1.2 Introduction to AFM lithography

AFM lithography has widely been used to fabricate nanostructures for future development of nanoscale devices such as magnetic tunnel junctions[9],[10], Josephson junctions[11],[12],[13], single electron transistors[14],[15], and field-effect transistors[16],[17], and so on. There are various types of AFM lithography method are currently developed such as anodic oxidation[18],[19],[20], dip-pen lithography[21], thermomechanical writing[22],[23], and indentation (direct mechanical lithography).

AFM anodic oxidation lithography which is operated contact and non-contact mode, changes the electrophysical properties of the sample surface as well as sample morphology. These changes came from the electrochemical reaction of sample and water in a humid atmosphere as shown in figure 1.1 (a). OH^- ions which are produced by the hydrolysis of the water, provide the oxidant for electrochemical reaction.

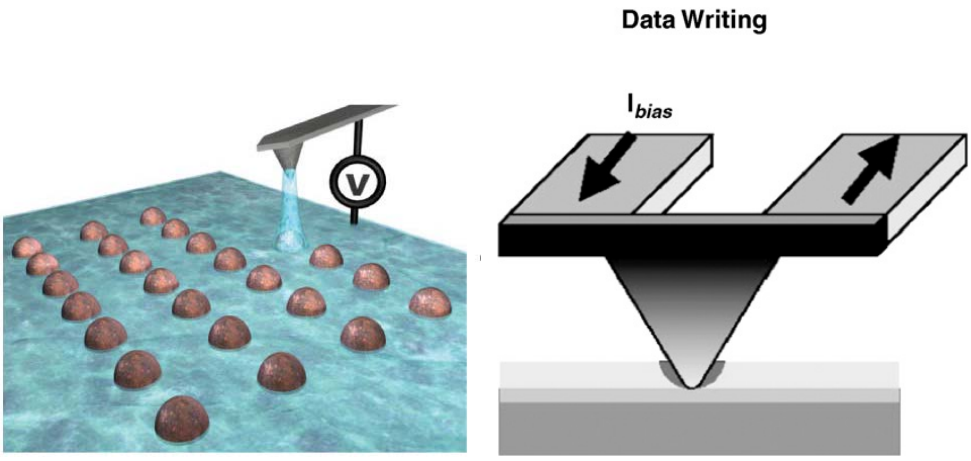

(a) (b)

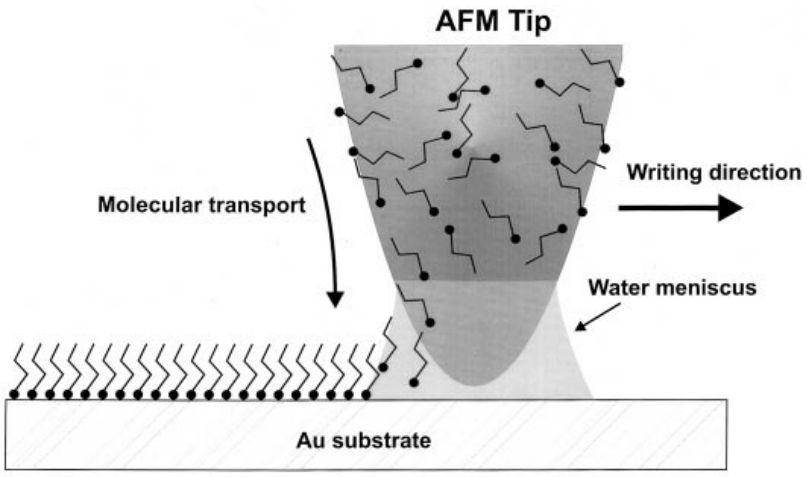

(c)

Figure 1.1 Schematic diagrams of the various types of AFM lithography, (a) anodic oxidation (Ricardo Garcia et al. Chem. Soc. Rev., 2006, 35, 29), (b) thermomechanical writing (X.N. Xie et al. Materials Science and Engineering 2006 R 54 1), and (c) dip-pen lithography (Richard D. Piner et. al. Science. 1999. 283, 661).

For example, oxidation process of the silicon surface can be written as:

$$Si + 4H^{+} + 2OH^{-} \rightarrow SiO_2 + 2H^{+}$$

Dip-pen lithography is one of AFM lithography methods, was developed by Richard D. Piner et. al. in 1999. The technology is a method of fabrication of nanoscale pattern using the method transferring the molecule to the substrate as shown in figure 1.2 (c). After the molecule is coated on to AFM tip, a nanoscale pattern can be created by the molecular transport from the tip to the substrate for a pattern. Dip-pen nanolithography, which is a useful method to fabricate nanoscale pattern, can be obtained below 30 nm of line width.

Thermomechanical writing for data storage using AFM lithography was developed by H. J. Mamin et. al. in 1992. This technique uses joule heating in a specially fabricated cantilever by micro-electromechanical systems technique as shown in figure 1.1 (b). The cantilever heated by current through the cantilever, creates a small size of data bits in polymer using a thermomechanical writing technology or deletes the data bits. The size of a data bit is approaching 20 nm using the technique.

AFM indentation nanolithography is a method where the AFM tip applies mechanical forces to deform the sample surface at a specified position in creating nanoscale patterns such as indentation holes and line grooves [13],[17],[24],[25],[26] as shown in figure 1.2. The size and form of the AFM tip apex and the magnitude of the applied force are critical to determining the size and the position of the patterns. In other words, the resolution of AFM indentation lithography is determined by the size of AFM tip radius. Hence, it is easy to fabricate nanoscale structure using AFM tip with a typical radius of less than 10 nm ~ 20 nm. In fact, there is a report that a line groove pattern of 7 nm width was fabricated on GaAS surface by C. K. Hyon et. al[27].

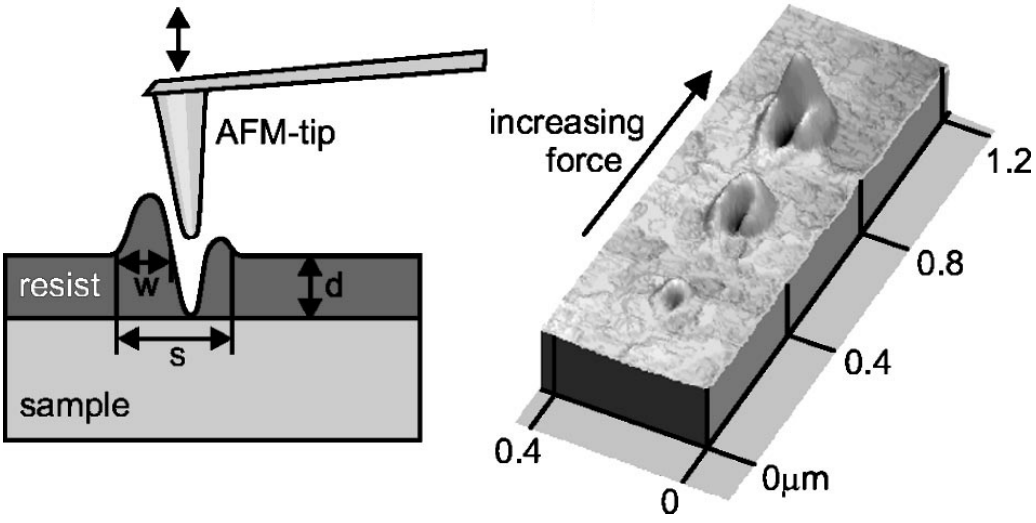

(a) **(b)**

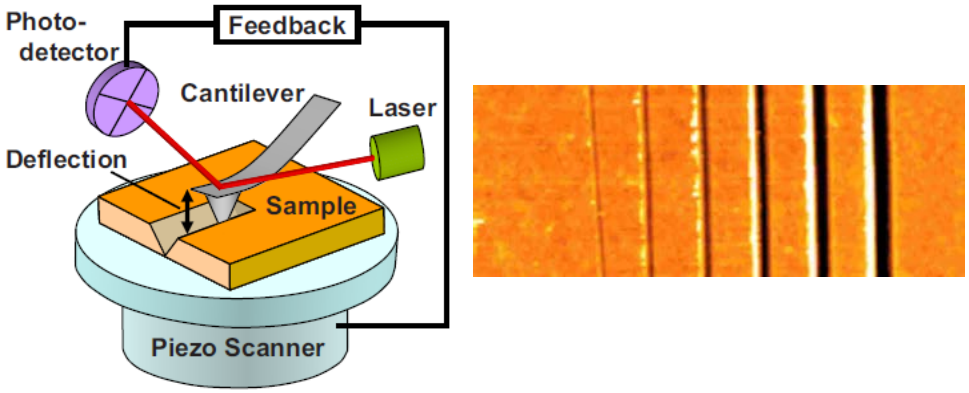

(c) **(d)**

Figure 1.2 Schematic diagrams of the AFM indentation lithography, (a) creating hole patterns, (b) AFM image of hole pattern (K. Wiesauer and G Springholz J. Appl. Phys. 2000. **88** 7289), (c) creating line groove pattern, and (d) AFM image of line groove pattern (Kazuya Miyashita et al J. Vac. Sci. Technol. B. 2009. **27** 953).

This indentation lithography method is very convenient method which is not required additional device (voltage or current source, molecular ink, specially fabricated cantilever, etc.). This method has advantages such as very easy alignment to the sample surface and absence of additional etching process depending on the type of AFM indentation. This method also can be applied to any substrate, regardless of the kind polymer. While nanostructures have been easily built by this AFM indentation nanolithography utilizing the sharp AFM tip, tip damage from the indentation process limits the number of patterns that one tip can make reproducibly. To overcome this limitation, special tips, such as diamond-coated tips, are occasionally used[10],[28]. Sometimes multi array cantilever is also used to improve of the low throughput which is one of the other disadvantages of AFM lithography[29],[30].

1.2 Outline

The thesis is composed of 5 chapters. Chapters 2 to 4 provide the main body of this thesis.

Chapter 1 presented the introduction of this thesis.

Chapter 2 discussed about the AFM indentation lithography on double-layer structure with minimal tip damage which is the main target of this work to improve reproducibility. This chapter is consisted of two sections. The first section presented AFM indentation on single and double-layer structure. We explained previous work

about AFM indentation on single-layer by other group. After that, we talked about the problems of these results, and explained methods introduced in order to improve it. In the double-layer indentation, we explained the advantages of this method, and compared other group's method with ours. In addition, we also explained the shape of the undercut which is referred to double-layer indentation, using the ZnO nanowire growth. The second section presented fabrication of the quantum dot and nanowire. The results of fabricated indentation pattern using the double-layer method as previously described are presented. Quantum dos, the final results of the hole indentation, are also presented. We explained about the consecutive-hole-indentation method by adjusting the distance between the holes with non-contact double-layer method we developed, and how to improve the reproducibility of line groove pattern. Nanowires, the final results of the line groove pattern, are also presented.

Chapter 3 discussed about the application of the AFM indentation lithography. This chapter is consisted of three sections. The first section presented electrical characteristics of gold nanowire with electrode. The gold nanowire was fabricated on the substrate with electrodes, which were made by standard photolithography methods, and then current-voltage characteristics were measured. Four different measurements of the current versus voltage characteristics of the nanowires measured by the two-terminal method, and we obtained the resistivities of the gold nanowires using this result. The second section presented the comparison of the AFM tip damage. For comparison, two line grooves of the same length (15 μm in length) and depth were made using the ploughing method and the consecutive-hole-indentation method by adjusting the distance between the holes. Then, a scanning electron microscopy (SEM) investigation was carried out on the used AFM tips. The AFM imaging was also carried out on single wall carbon nanotube (SWCNT), and radius of AFM tip was calculated using the tip convolution effect. The third section presented the removal of the bulge.

We explained how to remove the bulge previously developed in our laboratory, and how to remove the bulge containing the metal newly developed.

Chapter 4 discussed about the effect of indentation speed on pattern structures. This chapter is consisted of two sections. The first section presented the changes in the shape and depth of the indentation pattern according to the indentation speed. We explained how the depth and shape of pattern change depending on the indentation speed, and we were trying to understand of these changes using the rotation of AFM cantilever. The second section presented the changes in the substructure of the pattern according to the indentation speed. We explained how the substructure inside the pattern changes depending on the indentation speed, and we were also trying to understand of this change using stick-slip motion between the AFM tip and double-layer structure.

Finally, chapter 5 presented conclusion of this thesis.

Bibliography

[1] J. Fujita, Y. Ohnishi, Y. Ochiai, and S. Matsui, Appl. Phys. Lett. **68**, 1297 (1996)

[2] A. S. Chen, A. R. Neureuther, and J. M. Pavkovich, J. Vac. Sci. Technol. B 3, **148** (1985)

[3] C. Vieu, F. Carcenac, A. Pepin, Y. Chen, M. Mejias, A. Lebib, L. Manin-Ferlazzo, L. Couraud, H. Launois, Applied Surface Science **164**, 111 (2000)

[4] A Heuberger, J. Vac. Sci. Technol. B **6**, 107 (1988)

[5] D. J. D. Carter, A. Pepin, M. R. Schweizer, H. I. Smith, and L. E. Ocola, , J. Vac. Sci. Technol. B **15**, 2509 (1997)

[6] L. Bach, I. P. Reithmaier, A. Forchel, J. L. Gentner, and L. Goldstein, Appl. Phys. Lett. **79**, 2324 (2001)

[7] Stephen Y. Chou, Peter R. Krauss, Preston J. Renstrom, Science. **272**, 85 (1996)

[8] Yang Lu, Jian Yu Huang, Chao Wang, Shouheng Sun & Jun Lou, Nature Nanotechnology. **5**, 218 (2010)

[9] K Watanabe, Y Takemura, Y Shimazu and J Shirakashi, Nanotechnology, **15**. S556 (2004)

[10] Kazuya Miyashita, Shinya Nishimura, Takashi Toyofuku, and Jun-ichi Shirakashia J. Vac. Sci. Technol. B **27** 953 (2009)

[11] Takeshi Imamura, IEEE Trans. Appl. Supercond. **2** 84 (1992)

[12] Faucher, M, Fournier, T, Pannetier, B, Thirion, C, Wernsdorfer, W, Villegier, J C, Bouchiat, V, Physica C **368** 211 (2002)

[13] A A O Elkaseh, W J Perold, and V V Srinivasu J. Appl. Phys. **108** 053914 (2010)

[14] V. Bouchiat and D. Esteve Appl. Phys. Lett. **69** 3098 (1996)

[15] S. Luscher, A. Fuhrer, R. Held, T. Heinzel, K. Ensslin, W. Wegscheider, and M. Bichler, Journal of Low Temperature Physics, **118**, 333 (2000)

[16] P M Campbell, E S Snow, and P J McMarr 1995 Appl. Phys. Lett. **66** 1388 (2010)

[17] Yudong He, Huanli Dong, Tao Li, Chengliang Wang, Wei Shao, Yajie Zhang, Lang Jiang, and Wenping Hu Appl. Phys. Lett. **97** 133301 (2011)

[18] P M Campbell and E S Snow Semicond. Sci. Technol. **11** 1558 (1996)

[19] P Avouris, T Hertel, and R Martel Appl. Phys. Lett. **71** 285 (1997)

[20] Gwangmin Kwon and Kyeongkeun Ko Haiwon Lee et al. J. Vac. Sci. Technol. B **29** 011034 (2011)

[21] Richard D. Piner, Jin Zhu, Feng Xu, Seunghun Hong, and Chad A. Mirkin, Science. **283**, 661 (1999)

[22] H J Mamin and D Rugar Appl. Phys. Lett. **61** 1003 (1992)

[23] X.N. Xie, H.J. Chung, C.H. Sow, A.T.S. Wee, Materials Science and Engineering **R54** 1 (2006)

[24] K. Wiesauer and G Springholz J. Appl. Phys. **88** 7289 (2000)

[25] ChaeHo Shin, InSu Jeon, SeungHee Jeon, and Zheong G. Khim Appl. Phys. Lett. **94** 163107 (2009)

[26] Borislav Vasić, Markus Kratzer, Aleksandar Matković, Andreas Nevosad, Uroš Ralević, Djordje Jovanović, Christian Ganser, Christian Teichert and Radoš Gajić Nanotechnology **24** 015303 (2012)

[27] C. K. Hyon, S. C. Choi, S. W. Hwang, D. Ahm, Y. Kim, and E. K. Kim, Jpn. J. Appl. Phys., Part 1 **38**, 7257 (1999)

[28] Ampere A. Tseng, Jun-ichi Shirakashi, Shinya Nishimura, Kazuya Miyashita, and Andrea Notargiacomo J. Appl. Phys. **106** 044314 (2009)

[29] Hyo-Jin Nam, Young-Sik Kim, Caroline Sunyong Lee, Won-Hyeog Jin, Seong-Soo Jang, Il-Joo Cho, Jong-Uk Bu, Woo Beom Choi, Seung Woo Choi, Sensors and Actuators A: Physical, **134**. 329 (2007)

[30] Young Oh, Chulmin Choi, Kunbae Noh, Diana Villwock, Sungho Jin, Gwangmin Kwon, and Haiwon Lee, J. Vac. Sci. Technol. B **29**. 06FD03 (2011)

Chapter 2

AFM indentation on double-layer structure with minimal tip damage

The damage of AFM tip is need to reduce in order to the fabrication of reproducible pattern and structure, because once the tip apex is damaged, the width and depth of the indentation pattern will vary even if the same loading force is applied. The main reasons of the AFM tip damage are as follows: The first is that the interaction between the tip and sample; the second is that the contact between the tip and substrate at single-layer method; the last reason is that the lateral force applied on the tip in the sample. In this chapter, double-layer structure and consecutive-hole-indentation by adjusting distance between the holes were simultaneously applied to fabrication of nanostructure in order to reduce of tip damage of the second and third reason.

In this experiment and all subsequent experiments, the lateral speed of the AFM tip and the z direction speed of the AFM scanner were fixed to 5 μm/s during the indentation. PMMA (950k A2, Microchem, Japan) was spin-coated at 5000 rpm for 40 seconds on thermally grown 100 nm thickness of silicon dioxide on a 10 × 10 mm^2 size of silicon substrate, then baked in oven at 170 ℃ for 30 minutes.

The indentation was carried out using a commercial AFM (Albatross II, NanoFocus, Korea), and a commercial non-contact silicon cantilever (NSG30, NT-MDT, Russia) with a

tetrahedral shape. The cantilever has a force constant of 40 N/m and a resonant frequency of 310 ~ 320 kHz. Each experiment was conducted with a new tip. The loading force applied on the gold-PMMA surface by the AFM tip was 2 ~ 3.5 μN. All experiments were carried out at room temperature with a relative humidity of 40 ~ 60 %.

2.1 AFM indentation on double-layer structure

2.1.1 Single-layer structure

A single-layer structure is commonly used to fabricate nanostructure in AFM indentation lithography[1],[2],[3]. This single-layer indentation method could easily make nanostructures as shown in figure 2.1. However, the AFM tip could be easily damaged because the tip applies the force to the hard substrate directly while making indentations[2],[3],[4]. Because of this tip damage, it has disadvantages, such as poor reproducibility and low productivity in forming nanostructures. The ploughing method is another way to simply fabricate nanowires[3],[4], but the AFM tip also can be easily damaged because of the lateral force applied to it. For this reason, it is difficult to fabricate regular shape of dot as shown if figure 2.1 (b), and boundary of nanowire is not clear as shown in figure 2.1 (d) because of the polymer residue between the nanostructure and the substrate.

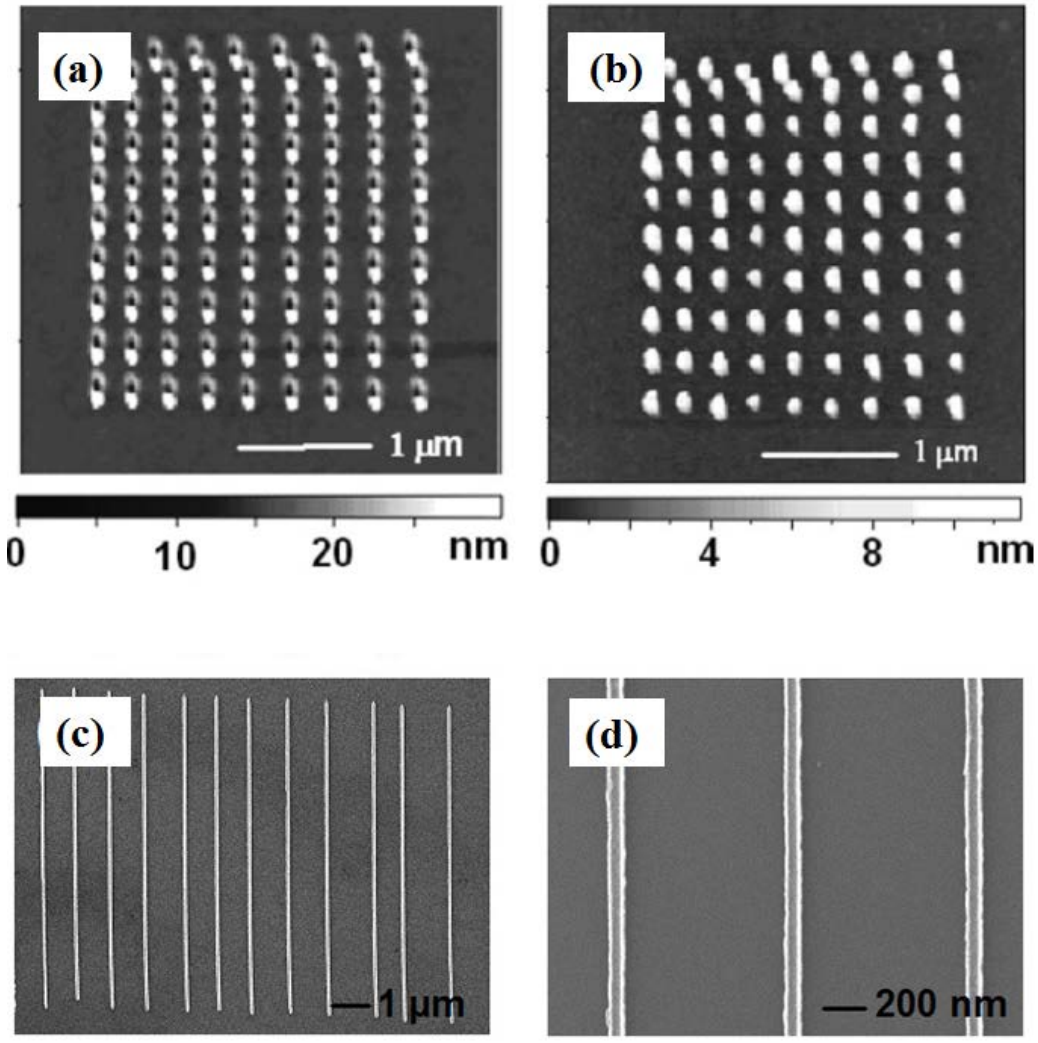

Figure 2.1 AFM images of (a) AFM image of an indentation pattern and bulge on PMMA, (b) AFM image of the corresponding gold nanodot array after lift-off (Ju-Hung Hsu et.al. 2004 J. Vac. Sci. Technol. B 22 2768), (c) the SEM image of the gold nanowires fabricated by plowing method, and (d) zoom image of (c) showing that the width is around 70 nm (Yu-Ju Chen et.al. 2005 Nanotechnology 16 1112).

To improve this direct contact problem between the tip and sample, we introduced an dry etching process at a single layer method as shown in figure 2.2. This method is that the indentation was carried out to avoid direct contact between the tip and sample as shown in figure 2.2 (a), and pattern was transferred to substrate by dry-etching process as shown in figure 2.2 (b). After that, we could get nanostructure by the metal deposition and the lift-off process as shown in figure 2.2 (c) and (d).

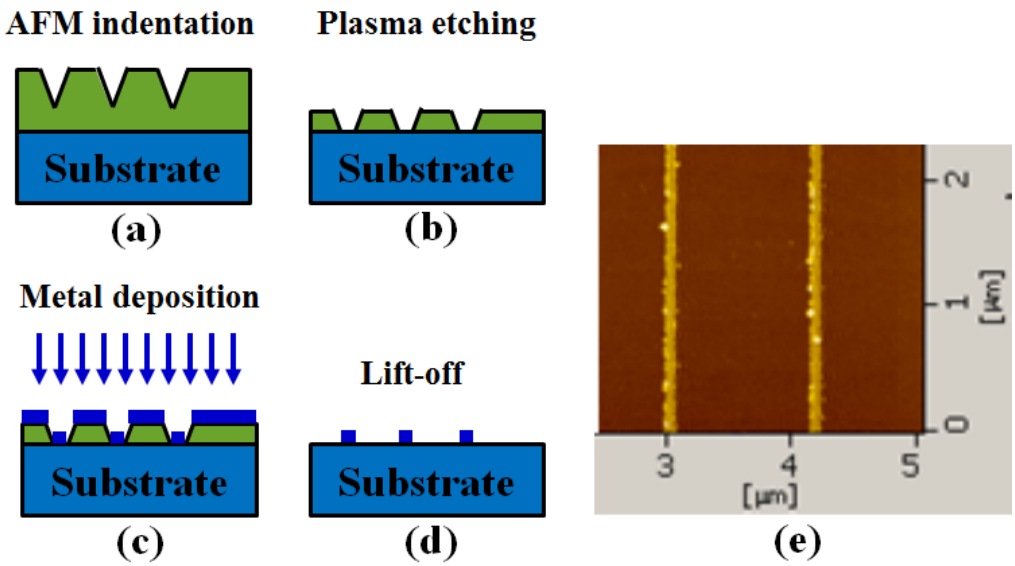

Figure 2.2 Schematic diagram of AFM indentation lithography on the single layer structure with dry etching process (a) AFM indentation on single layer, (b) dry-etching process, (c) metal deposition, (d) lift-off, and (e) AFM image of the nanowires fabricated by single layer process with dry etching process.

This method could reduce the tip damage because the tip and sample were avoided the direct contact. However, the boundary of the nanostructure is not clean as shown in figure 2.2 (e) because metal deposited on the edge of the pattern as well as on the substrate. If the PMMA thickness is too thin, it is difficult to control the etching condition because the etching rate of the conventional plasma etcher is too fast.

To address this issue, we employed a double-layer structure, which was proposed by S. Hu et.al. as an approach to minimize tip-wear[5]. In this experiment, we choose the gold which is known as soft metal, as a top layer metal in double-layer structure.

2.1.2 Double-layer structure

Gold was deposited onto the PMMA layer with the thickness of 15 ~ 20 nm as shown in figure 2. 3 (a). The thickness of the PMMA film and the root mean square values of the final gold-PMMA film were 80 nm and 0.45 nm, respectively. AFM indentation procedure on double-layer structure is as follows: The cantilever was first moved to a specified position on the double-layer sample surface in noncontact mode. After the feedback loop was disabled, the indentation process was performed. While the sample was raised to a preset height, the tip of the cantilever contacted and indented the sample surface. As soon as the sample reached the preset height, it retracted to the starting position using the piezotube.

These steps were repeated by moving the tip to other positions until a 40 × 40 or 20 × 20 quantum dot structure was created. Then, an isotropic O_2 plasma etching was applied to the

indented surface as shown in figure 2.3 (b) by PR Asher (V15-G, Plasma Finish, Germany) at base pressure 3.0×10^{-3} Torr, operation pressure 7.0×10^{-3} Torr, and plasma power 120 W for 70 ~ 80 seconds. The PMMA exposed to the plasma etchants was removed, while the PMMA beneath the indentation pattern formed an undercut due to the isotropic O_2 plasma etching. The undercut made it easy to remove the PMMA residue where the metal had been deposited. This guaranteed a clean contact without polymer residue between the nanostructure and the substrate, and made the lift-off easier. Although it was possible to deposit the metal in less than 70 seconds, a total minimum etching time of 70 ~ 80 seconds was needed to ensure the undercut formation. By this process, a metal mask having indentation holes and line grooves with the depth and width of a few tens of nanometers was fabricated.

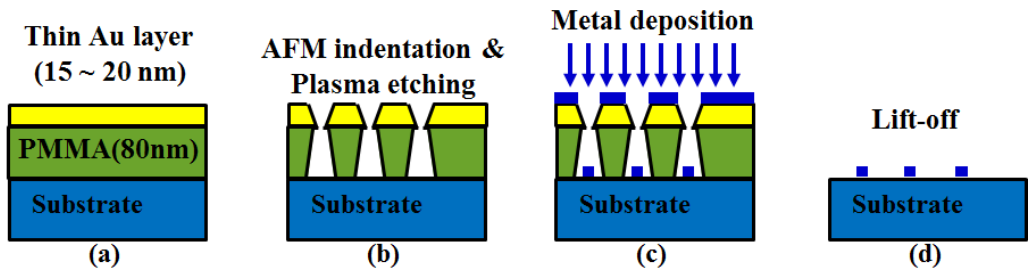

Figure 2.3 Schematic diagram of the AFM indentation lithography on the double-layer structure with dry etching process (a) AFM indentation on single layer, (b) dry-etching process, (c) metal deposition, (d) lift-off and (e) AFM image of the nanowires fabricated by single layer process with dry etching process.

We confirmed that undercut is formed in the double-layer structure using the ZnO growth. Figure 2.4 (a) shows the schematic diagram of ZnO growth method using wet chemical method. Wet chemical method is one of the method of ZnO (nanowire) growth which is a method that ZnO growth from the ZnO thin film when ZnO film was put in the specific solution.

The reaction processes in the solution can be expressed by the following equation[6]:

$$C_6H_{12}N_4 + 10H_2O \rightarrow 6HCHO + 4NH_3 \cdot H2O \quad (1)$$

$$Zn^{2+} + 4NH_3 \cdot H_2O \rightarrow [Zn(NH_3)_4]^{2+} + 4H_2O \rightarrow$$

$$Zn(OH)_2 + 4NH_4^+ + 2OH^- \quad (2)$$

$$Zn(OH)_2 \rightarrow ZnO + H_2O \quad (3)$$

In the aqueous solution of zinc nitrate, the methenamine decomposes to aldehyde and ammonia (equation (1)) in the weak acid condition. Then ammonia combines with Zn^{2+} to produce a large number of Zn^{2+} amino complexes in the solution. The Zn^{2+} amino complexes will be directly hydrolyzed (equation (2)), and ZnO can be formed on the glass substrate and vessel inter-surface through the decomposition reaction shown in equation (3).

In order to use this method, AFM indentation and plasma etching was performed after 100 nm thickness of ZnO thin film deposition. After that, the double-layer structure sample was put in the solution as shown in figure 2.4 (a). ZnO (nanowire) was grown at exposed ZnO thin film area by plasma etching under the certain conditions.

Figure 2.4 (b) shows the results of this experiment. We found that the ZnO growth is formed only in specific areas which are the undercut parts fabricated by plasma etching.

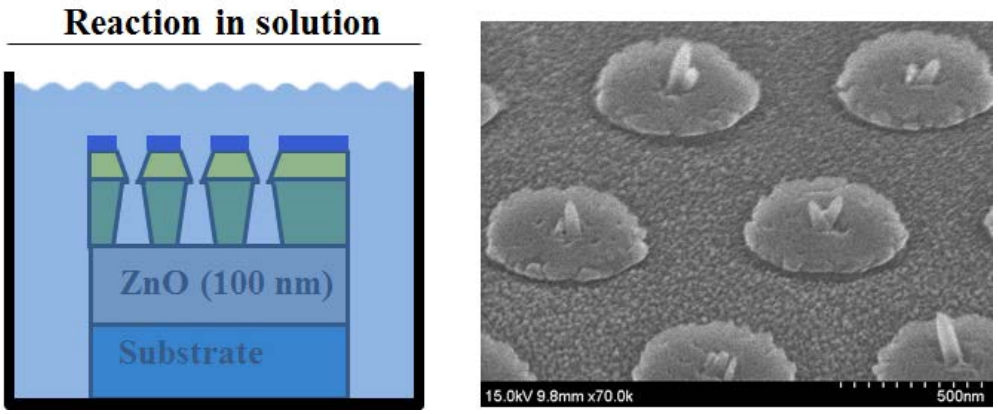

(a) (b)

Figure 2.4 (a) Schematic diagram of ZnO (nanowire) growth using the wet chemical method, and (b) FE-SEM picture of the ZnO (nanowire). ZnO (nanowire) was grew at exposed ZnO thin film area by plasma etching at the indented double-layer structure.

2.2 Fabrication of the quantum dot and nanowire

In our experiment, we used a double-layer structure to improve the reproducibility of a uniform nanostructure, which was made through the deposition of a soft thin metal layer on the polymer surface[5]. In the double-layer structure, the depth of the indentation pattern was set to be deeper than the thickness of the soft thin metal layer, but not deep enough for the tip to contact the substrate directly, thereby preventing the tip damage[2].

K. Wiesauer et.al showed that line groove pattern could be created by reducing the distance between the holes[7]. However, the fabrication of line groove pattern using the ploughing method also has limitations because of the tip damage from the single-layer structure on a hard substrate mentioned above. Once the tip apex is damaged, the width and depth of the indentation pattern will vary even if the same loading force is applied. The damaged tip apex makes it harder to create reproducible and uniform nanostructures using the conventional ploughing method.

In this section, we fabricated nanostructure using the newly developed method to reduce the AFM tip damage. Using the new method, we fabricated quantum dots and gold nanowires by creating indentation holes consecutively under the optimal adjustment of distances between neighboring holes. However, as an inherent drawback of this method, it requires extra processes such as metal deposition and plasma etching. While the extra processes add complexity and extra cost compared to a straightforward ploughing process, the method improves the uniformity and reproducibility of nanostructure. It also drops the cost of tip damage.

After the AFM indentation on the double-layer structure, gold used as the evaporation metal, was deposited with an e-gun evaporator (VI-43N, Anelva, Japan) at a thickness of 15 ~ 20 nm as shown in figure 2.3 (c). The base pressure was 3.0×10^{-7} Torr. The thickness of the gold was controlled using a thin film thickness monitor (XTC, Infilcon, Switzerland). Lastly, the lift-off procedure was conducted in acetone with ultrasonic cleaner for five minutes as shown in figure 2.3(d).

The final results of the AFM indentation lithography of the quantum dots and the nanowires were measured by non-contact mode AFM (SPA 400, Seiko, Japan) with a new cantilever of the same kind used for the indentation.

2.2.1 Quantum dots

Figure 2.5 (a) is the AFM image of the 40 × 40 indented hole pattern array with 6 μm × 6 μm of scan area, (b) is the close-up image of the marked area of (a) on the thin gold layer-PMMA structures. The distances between the indented holes range from 100 nm to 130 nm depending on the experimental conditions. 20 × 20 indented hole pattern array and its close-up image were shown in figure 2.5 (c) and (d). The depth of the indented hole is ~ 20 nm, which is deep enough to penetrate the thin gold film. Plasma etching, metal deposition, and lift-off process was performed using the indentation pattern of the double-layer structure fabricated by a method mentioned earlier as shown in figure 2.3 (b) to (d).

Finally, we were able to get a 40 × 40 gold quantum dot array result as shown in figure 2.6 (a) and (b), and a 20 × 20 gold quantum dot array result as shown in figure 2.6 (c) and

(d). The average full width at half maximum (FWHM) value of the gold quantum dot shown in the inset of figure 2.6 (b) was 42.4 nm ± 1.3 nm. The round shape of the gold quantum dot in figure 2.6 (b) indicates that the nanostructure is not directly related to the shape of the tetrahedral tip. This result suggests that the quantum dot was developed through diffusion process, which determines the shape and resolution of the quantum dot.

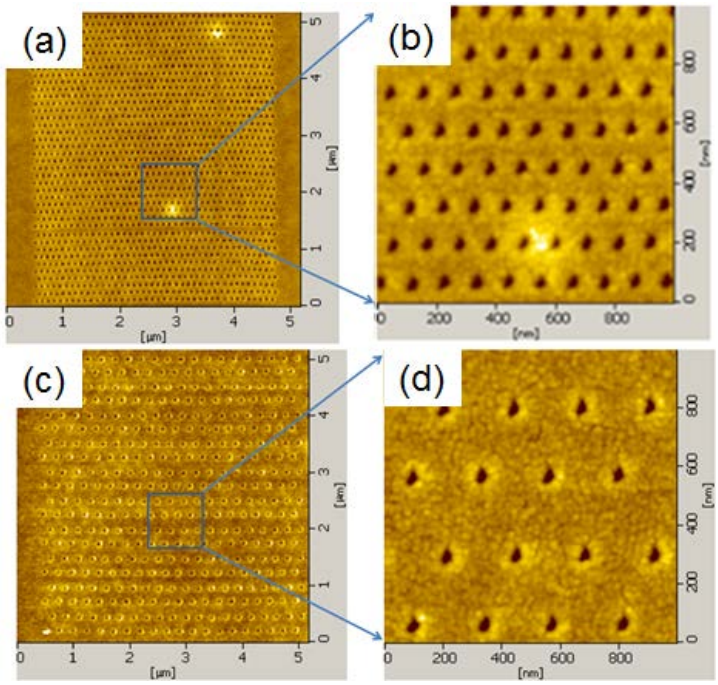

Figure 2.5 AFM image of (a) 40 × 40 indented hole pattern array, (b) close-up image of the marked area, (c) 20 × 20 indented hole pattern array, and (d) close-up image of the marked area.

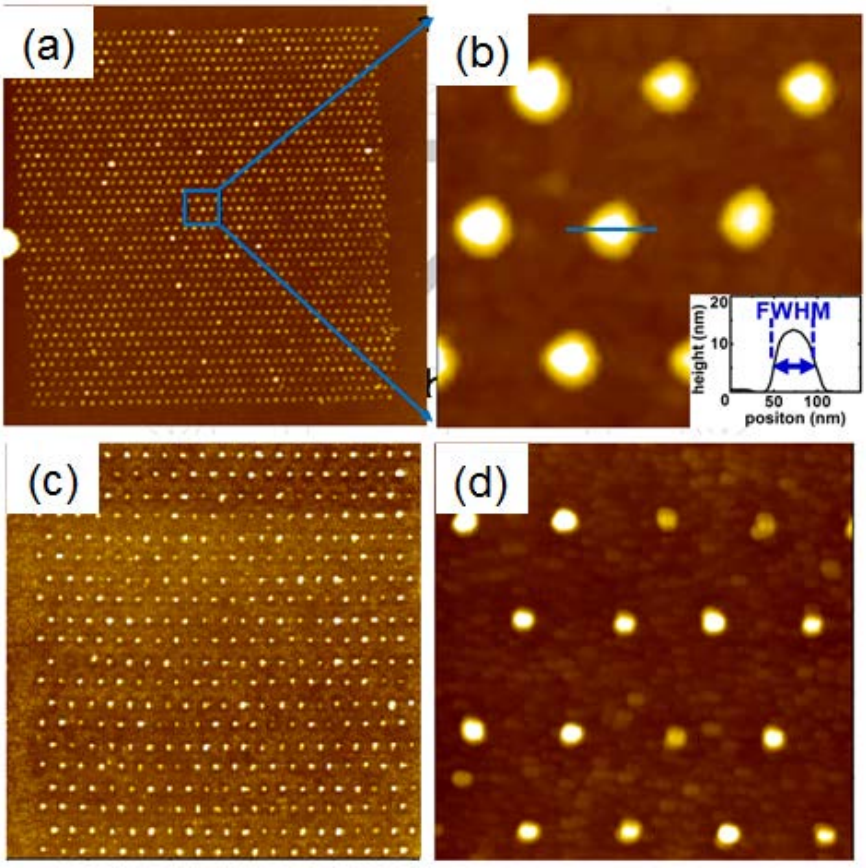

Figure 2.6 AFM image of (a) 40 × 40 gold quantum dot array result (scan area 6 μm × 6 μm), (b) close-up image of marked area (scan area 0.4 μm × 0.4 μm), (c) 20 × 20 gold quantum dot array (scan area 6 μm × 6 μm), and (d) close-up image of the marked area (scan area 1 μm × 1 μm).

2.2.2 Nanowires

The dot size in figure 2.6 (b) indicates that the quantum dots would connect if their distances were less than 50 nm. To test this idea, two nanowires were fabricated when the indentation hole distance was set at 50 nm. Contrary to our expectation, the two nanowires show that the dots are not connected completely as shown in figure 2.7. This result suggests that the gold film had not been completely removed between the two successive holes. The inset of figure 2.7 also shows that each dot was fabricated at intervals of ~ 50 nm, which is the indentation distance between the dent holes. This result indicates that the distance between the dent holes should be less than ~40 nm for the fabrication of a uniform nanowire.

When the hole distance was changed to 20 nm, we obtained two continuous line grooves. Figure 2.8 shows the two line grooves 15 μm in length and a close-up image of the marked area. This line groove pattern was made using the consecutive-hole-indentation method with a distance of 20 nm between the holes. The close-up image in figure 2.8 (b) shows that the two line grooves were uniformly fabricated in this hole distance.

When we repeated this experiment with hole distances less than 20nm, continuous line grooves were also obtained. The depth of the two line grooves is ~ 20 nm, which is also deep enough to penetrate the thin gold film.

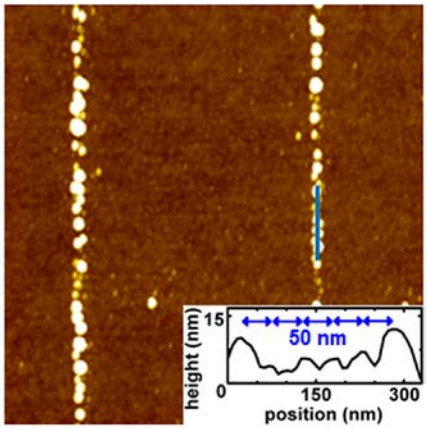

Figure 2.7 AFM image of gold nano dotted-line structure made by indentation with 50 nm distance between the holes (scan area 2 μm × 2 μm) (inset: cross section of the marked line).

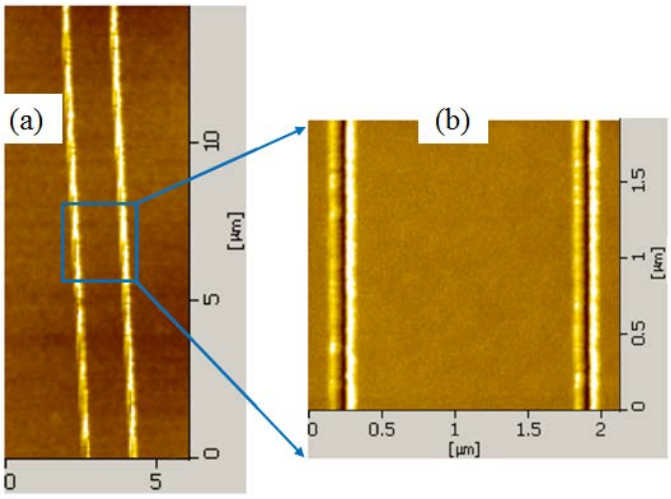

Figure 2.8 AFM images of (a) 15 μm length of line groove pattern, and (b) a close-up image of the marked area.

The AFM image (figure 2.9) shows a very uniform nanowire that was made using this method. The average FWHM value of the nanowire in figure 2.9 (b) was 63.1 nm ± 1.9 nm over 20 consecutive sectional profiles along the line grooves at intervals of 200 nm (figure 2.9 (c)). As a result, we found that the control of the distance between the holes is important to fabricating a uniform nanowire because adjusting the hole-hole distance minimized the tip damage by reducing unnecessary indentation. In addition, we could see that the boundary problem in figure 2.2 (e) was solved using the double-layer structure.

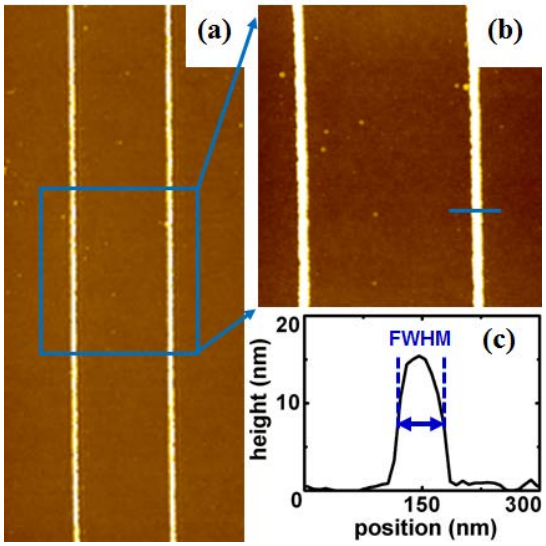

Figure 2.9 (a) AFM image of gold nanowire (scan area 3 μm × 6.5 μm), (b) close-up image of the marked area in (a) (scan area 2 μm × 2 μm), and (c) cross section of the marked line in (b).

Bibliography

[1] Y.-J. Chen, J.-H. Hsu, and H.-N. Lin, Nanotechnology **16**, 1112 (2005)

[2] C. Martín, G. Rius, X. Borrisé, and F. Pérez-Murano, Nanotechnology **16,** 1016 (2005)

[3] Ju-Hung Hsu, Chun-Yu Lin, and Heh-Nan Lina J. Vac. Sci. Technol. B **22** 2768 (2004)

[4] Yu-Ju Chen, Ju-Hung Hsu and Heh-Nan Lin Nanotechnology **16** 1112 (2005)

[5] S. Hu, A. Hamidi, S. Altmeyer, T. Köster, B. Spangenberg, and H. Kurz, J. Vac. Sci. Technol. B **16,** 2822 (1998)

[6] WEI Su-feng, JIANG Qing, and LIAN Jian-she, Trans. Nonferrous Met. Soc. China **18**, 1089 (2008)

[7] K. Wiesauer and G Springholz J. Appl. Phys. **88** 7289 (2000)

Chapter 3

Application of the AFM indentation lithography

3.1 Electrical characteristics of gold nanowire

A gold nanowire was fabricated under the same condition as the previous experiment in figure 2.9, and was connected to the electrodes on the substrate as shown in figure 3.1 (a) to study its electrical characteristics. Even if the height of the sample surface is different as shown in figure 4.1, nanowire could fabricated by consecutive-hole-indentation method. This is because the AFM tip is moving in non-contact mode with the feedback during the indentation.

The electrode was fabricated by standard photolithography. The distance between the electrodes was about 10 μm or 5 μm, and the height of the electrode was about 40 nm [oblique line area in figure 3.2 (a)]. Figure 3.2 (b) shows four different measurements of the current vs. voltage characteristics of the nanowires measured by the two-terminal method.

We obtained the resistivities of the gold nanowires using this result by making three assumptions as follows: The first is that the contact resistances (R_C) between the electrodes and the nanowire are the same at both ends; The second is that the size of the contact

resistance is only inversely proportional to the area between the nanowire and electrode; The last assumption is that the circuit resistance is negligible except for the nanowire resistance (R_{NW}) and the contact resistance between the nanowire and electrode. According to the first and third assumptions, the total resistance of the system (R) is written as follows:

$$R = 2R_C + R_{NW} \tag{1}$$

Since the nanowire resistance is proportional to the ratio between the length and cross section area of the nanowire, it is written as follows:

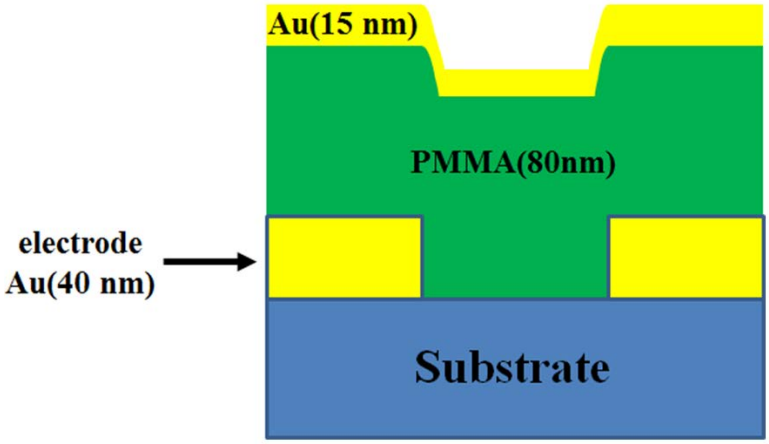

Figure 3.1 Schematic diagram of the sample structure for measurement of the electrical characteristics of the gold nanowires.

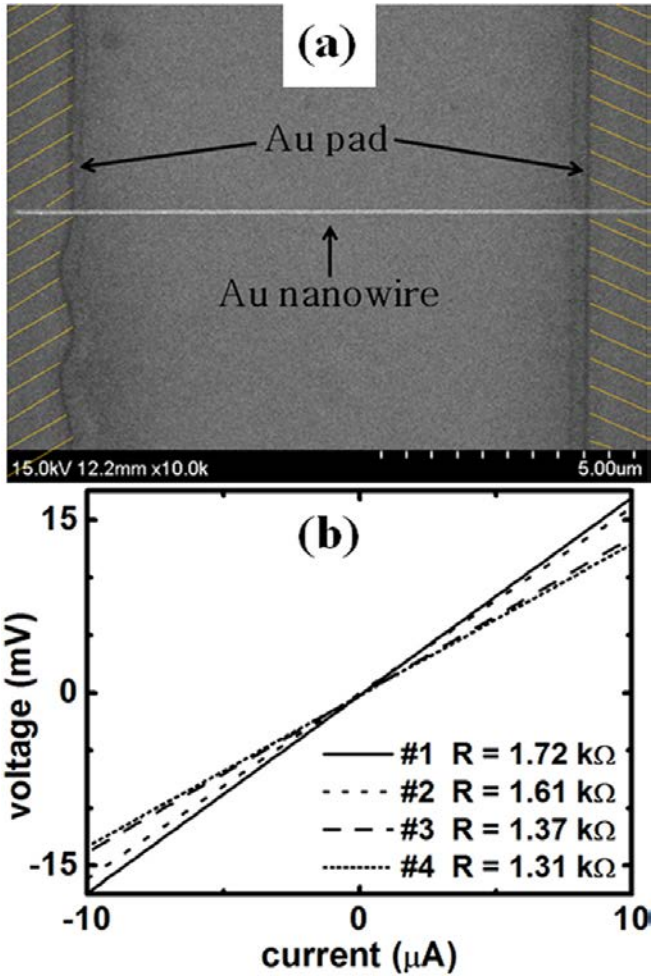

Figure 3.2 (a) FE-SEM picture of gold nanowire made on prefabricated electrode (oblique line area), and (b) voltage graph as a function of the electric current of gold nanowires. The length, width, and height of the nanowires are as follows. #1: 10.4 μm, 63 nm, and 21 nm, #2: 10.2 μm, 62 nm, and 21 nm, #3: 5.2 μm, 49 nm, and 20 nm, and #4: 5.2 μm, 48 nm, and 20 nm, respectively.

$$R_{NW} = \rho \frac{l}{w \times h} \tag{2}$$

where l, w, and h are the length, width, and height of the nanowire, respectively. The proportional constant ρ corresponds to the electrical resistivity. According to the second assumption, the contact resistance is written as follows:

$$R_C = \frac{C}{w \times h} \tag{3}$$

where C is a constant. The combination of the equations (2) and (3) with the equation (1) leads to the following equation:

$$R = 2\frac{C}{w \times h} + \rho \frac{l}{w \times h} \tag{4}$$

As equation (4) has two unknowns, C and ρ, two equations are required to determine them. The two equations were set up by choosing two nanowires, one from two 10 μm nanowires and the other from two 5 μm nanowires in figure 3.2 (b). The dimensional information on length, width, and height of each nanowire was obtained from AFM sectional profiles (see the caption of figure 3.2 (b)). The information of resistance R was found from the slope, as shown in figure 3.2 (b). The coupled equations were solved to determine ρ and C. We repeated these steps for all four possible pairs to find the average value for comparison with the literature value. The standard deviation was also calculated to find the uniformity of both ρ and C. The ρ and C were averaged to be

$(1.73 \pm 0.19) \times 10^{-7} \Omega m$ and $(1.99 \pm 0.65) \times 10^{-13} \Omega m^2$, respectively, for all four analyses. This resistivity we obtained is very excellent value than other group's experimental results[1]. The electrical resistivity of the gold nanowire obtained is seven times higher than that of the bulk gold, $2.44 \times 10^{-8} \Omega m$, found in literature[2].

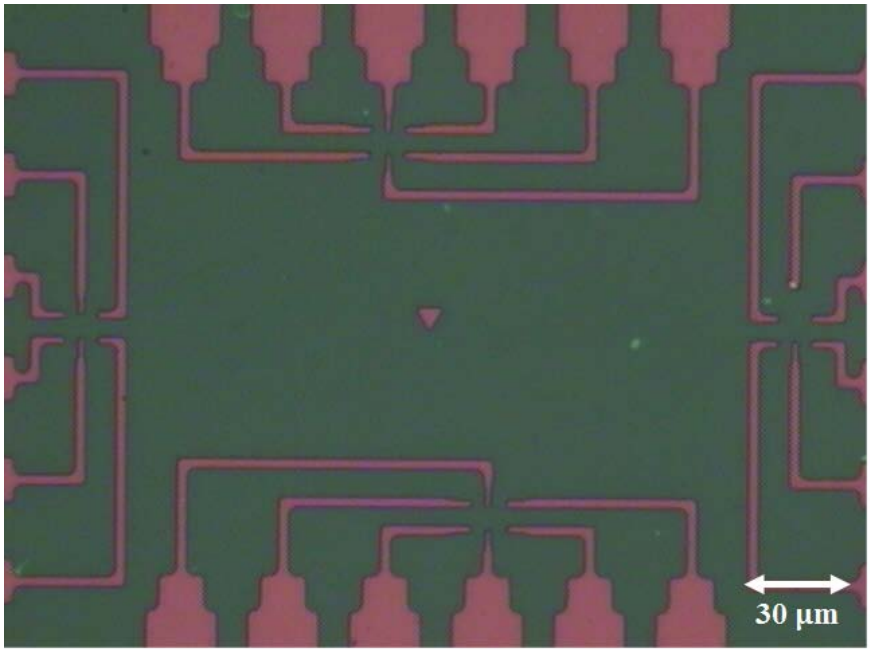

Figure 3.3 Optical microscopy image of electrode used in this experiment. Some part of the calculated value of the contact resistance is seem to be the resistance of the electrode itself.

This result suggests that the confined geometry of the nanowires increases the electrical resistivity significantly. Using the equation (3) and the constant C, the contact resistances are calculated to be 152 ± 50 Ω and 205 ± 67 Ω for the 10 μm and 5 μm nanowires, respectively. The total contact resistance $2R_C$ takes 18 % (= 304 Ω /1665 Ω) of the total resistance for the 10 μm nanowires. In other words, the nanowire resistance R_{NW} takes more than 82% in our experiment, which is dominant over the total contact resistance $2R_C$ in the total resistance R of the nanowires. By the way, we know that the assumptions mentioned above could be wrong. For example, we completely ignored the circuit resistance except for the nanowire and contact resistance. But, it is not true. When the size of an electrode is small, we have to consider the resistance of electrode itself.

Figure 3.3 shows the optical microscope picture image of the electrode used in this experiment. The resistance of the thin electrode as shown in figure 3.3 is calculated about 60 Ω using equation (2) (the gold resistivity value was used the value of the bulk gold[2].) This resistance value of the electrode is approximately 40% of the average contact resistance value, 152 Ω. Considering the resistance of electrode itself, the total contact resistance is about 11% of the total resistance. Therefore, we may think that the actual contact condition would be better than in previous thought.

The standard deviation is 11% (= $(0.19\times10^{-7}$ Ωm) / $(1.73\times10^{-7}$ Ωm)) for the electrical resistivity, while it is ~30% (= 50 Ω /152 Ω) for the contact resistance. This higher variation in the contact resistance may be due to the irregular interfaces (and thus the cross section area) at the boundaries of gold pads in figure 6(a). Since $\Delta R_{NW}/R_{NW}=-\Delta w/w$ from equation (2) assuming that ρ, l and h are constant, the ~10% variation in $\Delta R_{NW}/R_{NW}$

corresponds to the same variation in the width, or Δw/w. This result suggests that our double-layer indentation method is capable of creating uniform and reproducible nanowires up to 90%, consistent with the AFM topographic result (see figure 5(a) and 5(b)). The efficient removal of polymer residues by the dry etching process may contribute to the observed uniformity and reproducibility of the gold nanowires. The dry etching process also contributed to the clean contacts between the nanowire and electrodes. Another aspect worth mentioning is that the AFM feedback during the lateral tip movement between the successive indentations contributed to the result by enabling the indentation method to make indentation patterns with the same depth even with the height variations of the sample surface.

3.2 Comparison of the AFM tip damage

We investigated the damage to the AFM tip to compare the consecutive-hole-indentation method and the ploughing method. The loading force of the AFM tips when creating the line grooves was applied to get same indentation depth. The AFM tip was not contact with the substrate in both cases in order to verify the difference in AFM damage caused by lateral force. The tip damage was investigated after the fabrication of line grooves 15 μm in length using each method, where each experiment was conducted with a brand new tip.

The SEM measurements show that that the tip diameter used in the ploughing method as shown in figure 3.4 (a) was approximately two times bigger than that used in the consecutive-hole-indentation method as shown in figure 3.4 (b). This result indicates that the consecutive-hole-indentation method caused less damage to the tip than the ploughing method.

We investigated the damage to the AFM tip by using another method at this time. Line groove pattern was fabricated by the same condition as mentioned earlier, and then, SWCNT smaller than AFM tip apex was imaged by used AFM tip. The AFM tip radius was estimated using the tip convolution effect as shown in figure 3.5 (d).

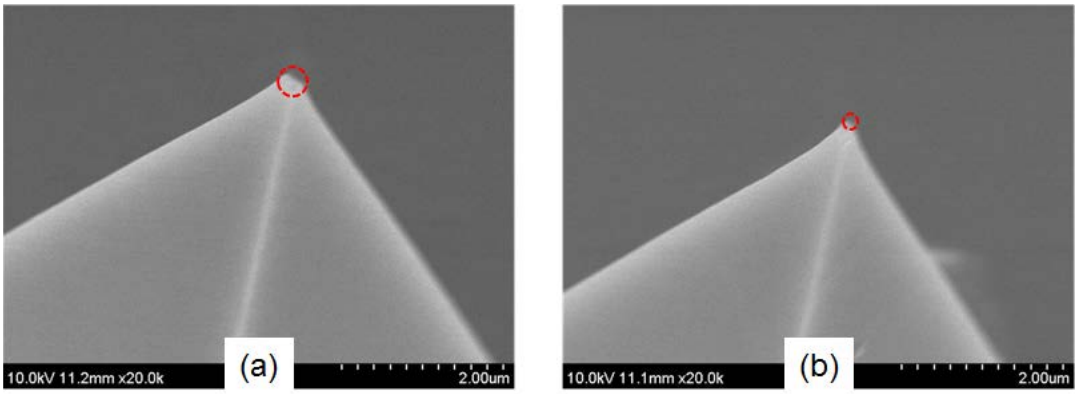

Figure 3.4 FE-SEM pictures of used AFM tip as (a) ploughing method and (b) the consecutive-hole-indentation method.

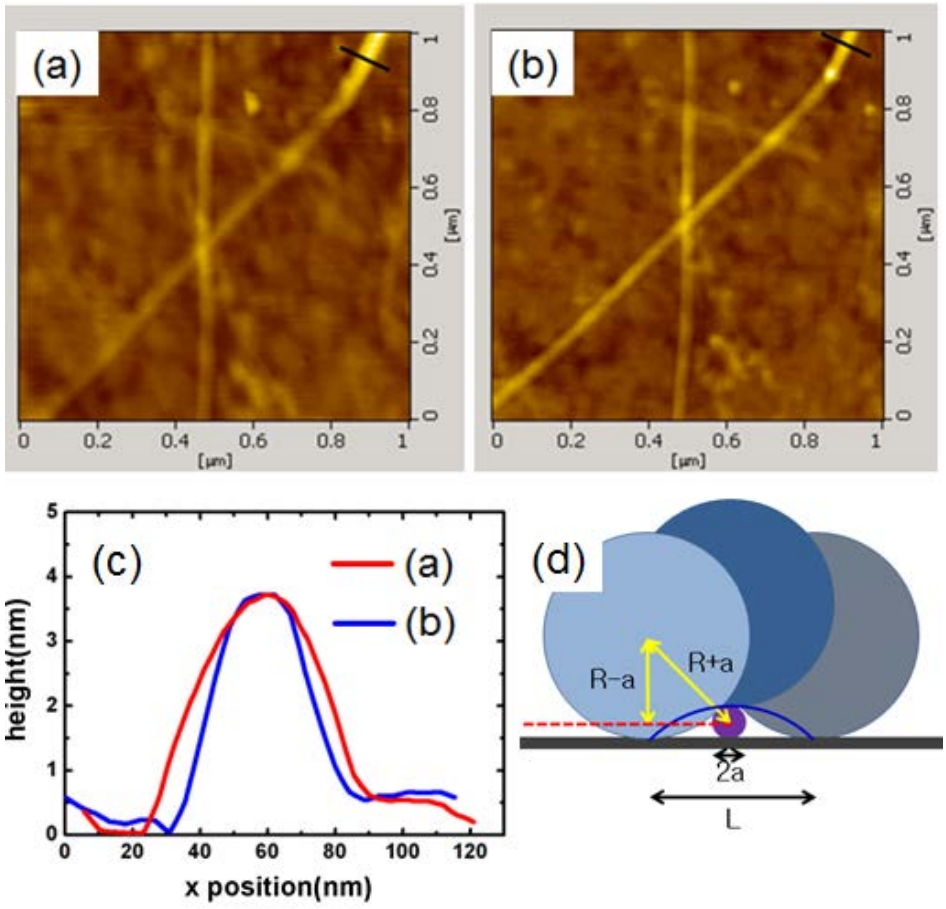

Figure 3.5 AFM images of SWCNT used AFM tip as (a) ploughing method, (b) the consecutive-hole-indentation method, (c) cross sectional profile at the same position (black bar in the AFM image), and (d) simple model of tip convolution effect.

The relation between the measured line width of the nanostructure and the raius of the AFM tip can be written as follows:

$$(R + a)^2 - (R - a)^2 = (L/2)^2$$

$$\rightarrow \quad R \propto L^2 \tag{5}$$

where a is a half width of nano structure, R is a tip radius, and Lis a measured line width of a nanostructure using AFM tip. We could get the same result by substituting the measured value of line width to the equation (5).

Figure 3.6 shows the result to test the durability of the AFM tip. 40 × 40 gold quantum dot was continuously fabricated by one AFM tip in order from (a) to (d) as shown in figure 3.6. This experiment is a confirmation experiment that how many quantum dot can make by one AFM tip. The same loading force was exerted on the AFM cantilever in this experiment. We could know that the fourth result, (d), of quantum dot was not created properly (quantum dot was fabricated from left to right of AFM image.). We finally could know that one AFM tip could make 5,000 ~ 5,500 of quantum dots without change of fabrication condition such as loading force.

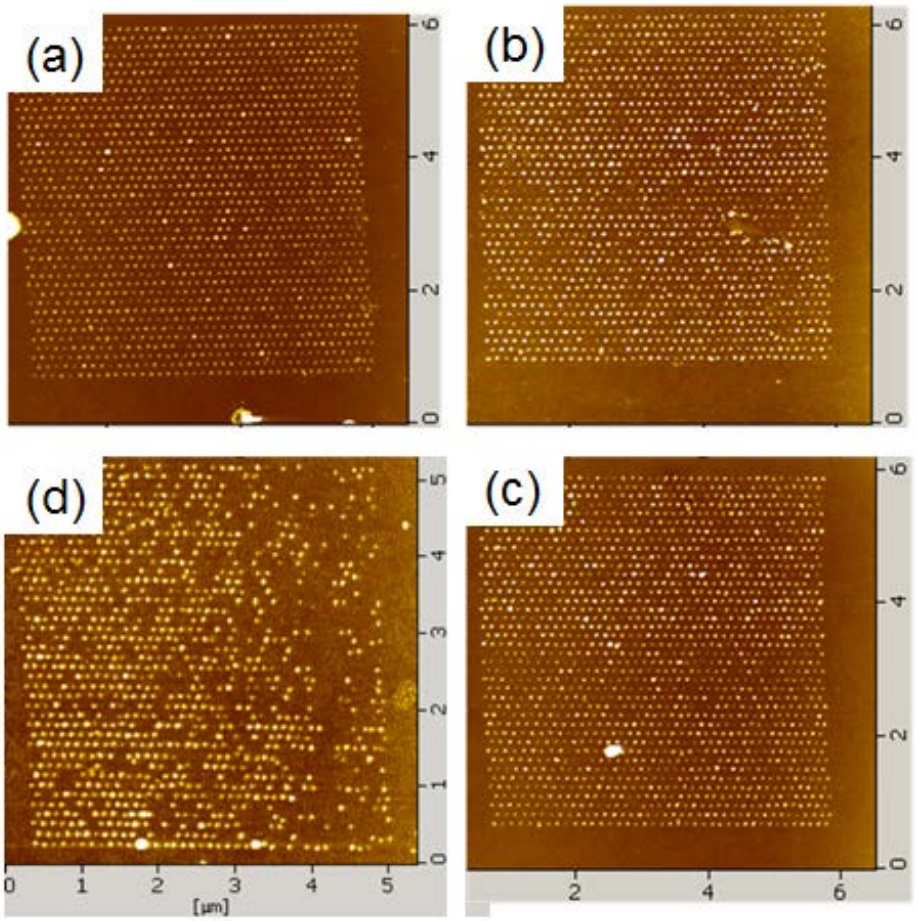

Figure 3.6 Durability test of the AFM tip. AFM images of 40 × 40 gold quantum dot continuously fabricated by one AFM tip with the same loading force (a → b → c → d).

3.3 Removal of the bulge

If the distance between the indentation pattern become closer or the pattern has overlap part like a cross line, the indentation hole or line groove pattern is blocked by the bulge. The bulge removing is required to solve this problem such as the previously mentioned earlier..

3.3.1 Introduction of bulge removal on single-layer

Figure 3.7 shows that the result of bulge removal in single layer (PMMA) performed by our group[3]. This method is a method to remove PMMA bulge using a mixture of de-ionized (DI) water and isopropanol (IPA). To remove the PMMA bulge, the sample is placed in properly mixed solution of a DI water and IPA, and then applied the ac or dc electric field under ambient conditions. The images in figure 3. 5 indicate that a bulge was completely removed when a 1:5 mixed solution of DI water and IPA, respectively.

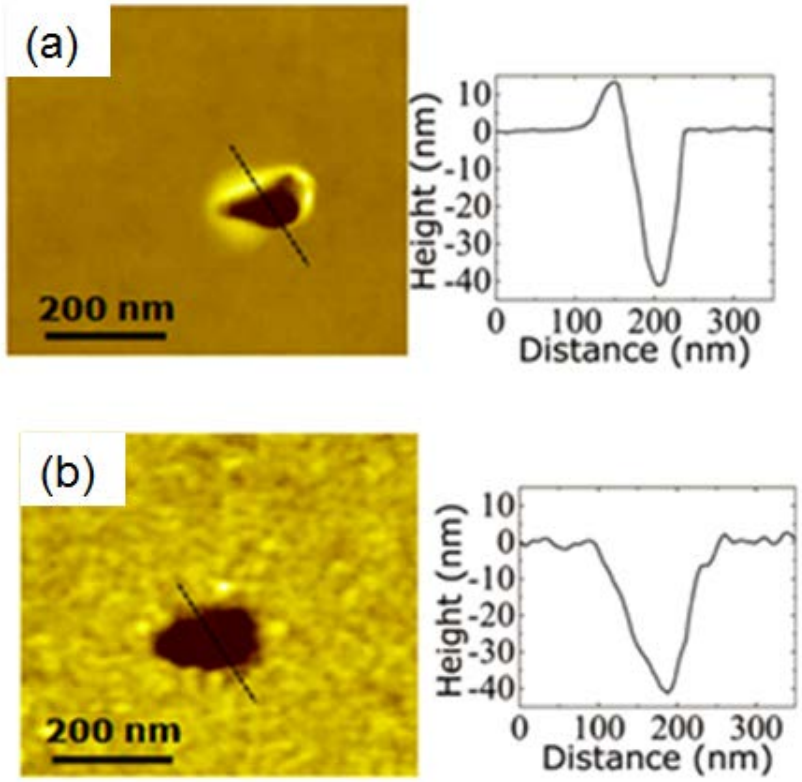

Figure 3.7 (a) Dent hole image and dent hole height profile after AFM indentation of PMMA (950 K A2). Cross-sectional height profile shows dent hole width of 71.4 nm, dent hole depth of 41.2 nm, and rim bulge height of 12.9 nm. (b) Dent hole image and height profile after treatment with DI water and IPA (ratio of 1:5, respectively) in a 10^4 V/m electric field for 10 min. Cross-sectional view shows dent hole width of 144.7 nm and depth of 41.9 nm. Note that the bulge on the dent hole rim was removed (ChaeHo Shin et.al Appl. Phys. Lett. 94 163107 (2009)).

3.3.2 Removal of bulge containing the metal

The bulge of the double-layer structure is contained metal like gold. The bulges containing the metal are not removed by the method described earlier, because the metal inside the bulge stuck with the metal of top layer. So, we were changed the double-layer structure in order to remove the metal bulge as shown in figure 3.8. In this structure, the metal bulge created by the indentation goes up on the top layer of PMMA. In other words, ultra-thin PMMA layer prevent metal bulge from directly sticking with metal. Of course, this kind of bulge is not removed by the method described earlier, because the metal and metal stick.

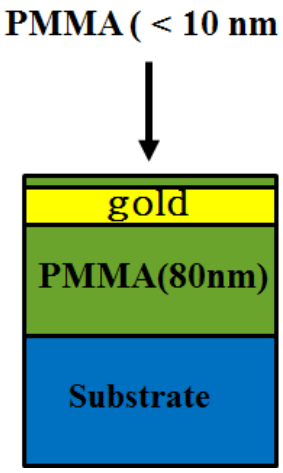

Figure 3.8 Schematic diagram of newly introduced structure. Ultra-thin PMMA layer was coated on the gold layer.

To solve this problem, we introduced ultrasonic vibration in the solution same as mentioned earlier (sonication for 30sec with 1:5 solution of DI water and IPA). We could find that the metal bulge is removed by ultrasonic vibration within a reasonable time. It seems to be metal bulge washed out with ultra-thin PMMA layer. Figure 3.9 shows the examples of removed metal bulge. We could easily know that the metal bulge is removed.

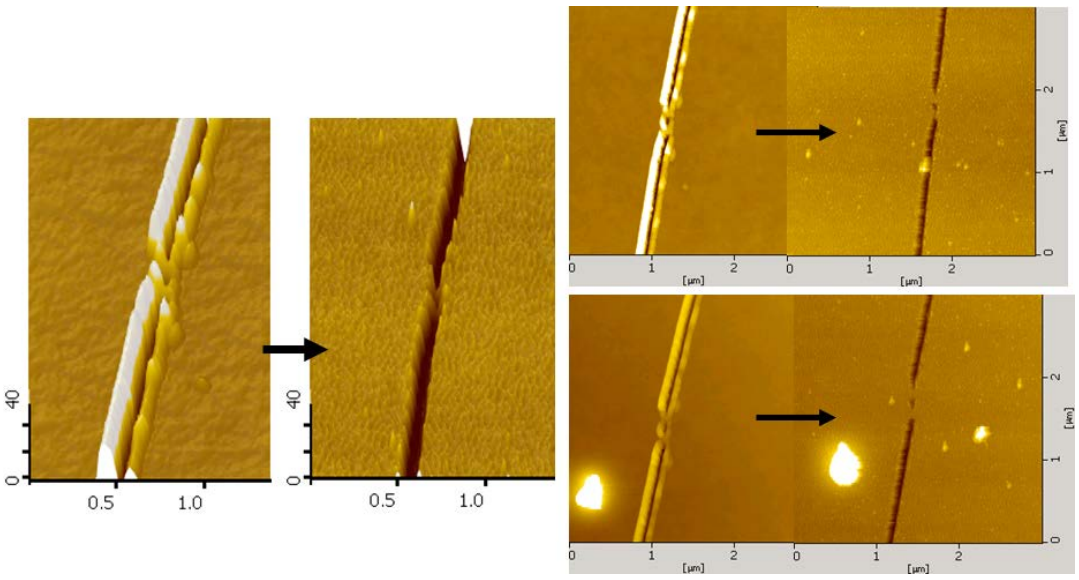

Figure 3.9 Examples of removal of bulge containing metal. The left images of each figure are the image of after the indentation, and the right images of each figure are the image of after the sonication in the solution.

Bibliography

[1] J.-H. Hsu, C.-Y. Lin, and H.-N. Lin, J. Vac. Sci. Technol. B **22,** 2768 (2004)

[2] J. D. Cutnell and K. W. Johnson, Physics (J. Wiley, Hoboken, 2004), 6th edition, pp. 582

[3] ChaeHo Shin, InSu Jeon, SeungHee Jeon, and Zheong G. Khim Appl. Phys. Lett. **94** 163107 (2009)

Chapter 4

Effect of indentation speed on pattern structures

The delicate nanoscale indentation structure is determined by the complex deformation process of the double-layer film under the sharp AFM tip. The structure at the faster tip speed would be especially interesting in order to improve the throughput of AFM lithography. So far, however, any systematic approach to the understanding of the dynamic aspect of the interactions between the tip and this inhomogeneous structure has not been reported. The shortcoming of this approach appears to be due to the fact that classical elastic continuum theories such as the Hertzian model[1] are not easily applied to this type of data sets. Hence, the understanding of the speed-dependent indentation process must include the classical elastic terms. Here, to understand the dynamic aspect of the nanoindentation process, we investigated how the indentation pattern depends on the tip approach and retraction speed using a double-layer structure.

We chose gold and PMMA as the double-layer on an oxidized silicon surface. The indentation was performed by a commercial AFM (Albatross II, NanoFocus, Korea). The cantilever was a commercial noncontact silicon cantilever (NSG30, NT-MDT, Russia) with a tetrahedral shape as shown in figure 4.1 (a). The cantilever had a force constant and resonant frequency of 40 N/m and 320 kHz, respectively. After turning off the z-feedback,

the AFM indentation was carried out by raising the AFM z scanner to a set height that was sufficient to generate enough force for the tip to penetrate the gold film[2]. It is important to note that to avoid any tip-wear observed by an earlier study for single-layer[3], the set height should not be high enough to make direct contact with the substrate. The indentation depth in the double-layer was set to be 40-50nm, which is approximately 2 ~ 3 times larger than the thickness of the thin gold layer, 15 ~ 20nm. The scanner was used to create such indentation depths by traveling. After that, the scanner came back to the height of the starting point of the indentation process. This process was repeated at a new position of the sample, where the tip was moved using noncontact mode AFM imaging with the z-feedback on. The indentation speed was controlled by speed change of AFM z scanner.

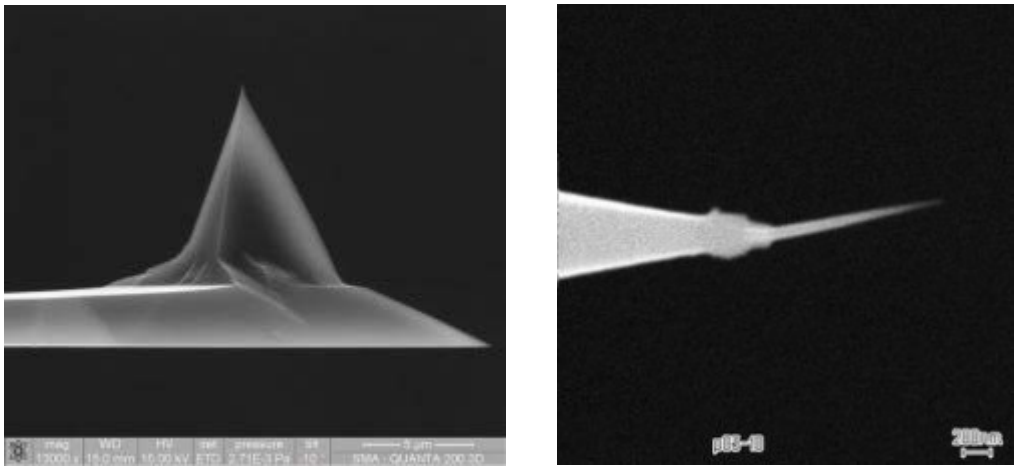

(a) (b)

Figure 4.1 FE-SEM pictures of (a) a NSG30 non-contact probe used in indentation, and (b) an whisker type high aspect ratio probes used in measurement of indented pattern.

Finally, the indentation patterns were measured by non-contact mode AFM (SPA 400, Seiko, Japan) with a whisker type high aspect ratio tips (NSC05, NT-MDT, Russia) as shown in figure 4.1 (b)[4]. The standard length of high aspect ratio tip is 1.0 ± 0.2 μm with inclination angle 10 degrees.

Figure 4.2 (a), (b), and (c) show the patterns indented at speeds of 0.2 μm/s, 1 μm/s, and 5 μm/s, respectively. Each hole in figure 4.2 (a) has the shape of a distorted half-circle. The sectional profile in figure 4. 2 (d), taken across the solid line in figure 4.2 (a), shows the substructures in the inside pattern (as marked with blue arrows). The average indentation depth and pattern length of y direction of the hole pattern was 34.2 nm ± 2.0 nm, and 126.6 nm ± 3.9 nm, respectively. When the indentation speed was increased to 1 μm/s, the pattern structure remained almost the same as shown in figure 4.2 (b). The sectional profile in figure 4.2 (e) still shows substructures. The indentation depth slightly increased to 36.1 nm ± 1.2 nm by 5.6 %, but pattern length of y direction did not change within the error range. When the indentation speed was increased to 5 μm/s, the shape of the structures was changed from distorted half-circles to triangles as shown in figure 4.2 (c). As the tip has a tetrahedral shape, the observed structures appeared to come from the AFM tip. Furthermore, the sectional profile in figure 4.2 (f) shows that the substructures had disappeared. In addition, the indentation depth was increased to 42.2 nm ± 1.1nm by 23 %, but pattern length decreased to 113.1 nm ± 4.6nm by 11 %.

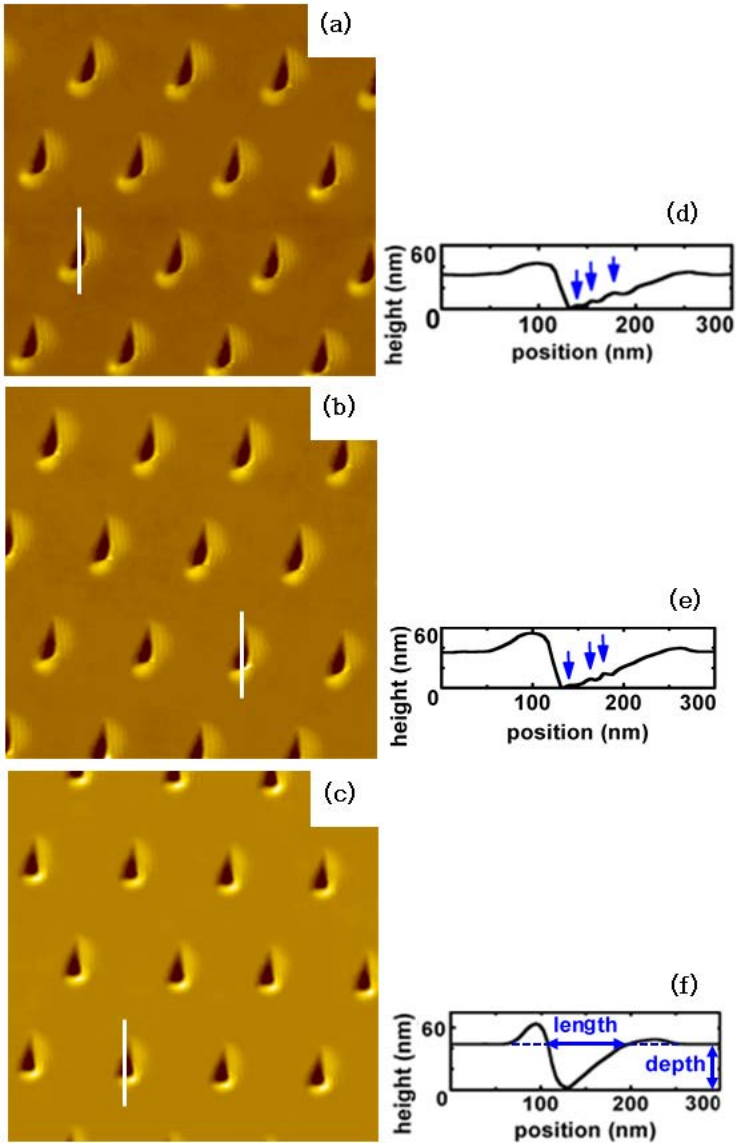

Figure 4.2 (a), (b), and (c) AFM images of dent hole patterns according to the change of indentation speed, which is 0.2 μm/s, 1.0 μm/s and 5 μm/s, respectively (scan area 1.2 μm × 1.2 μm), (d), (e), and (f) cross sections of marked line in (a), (b), and (c), respectively.

Figure 4.3 shows that the comparison of AFM image and cross sectional profile of indentation pattern measured by new tip of same kind of using indentation experiments and high aspect ratio tip. As you can see cross sectional profile, the substructure in the inside pattern may be better analyzed when measured by high aspect ratio tip. This results indicates that when we measure the indentation pattern, use of the special tip such as the high aspect ratio tip or super sharp tip is more advantageous than use of the normal tip (even if using the new tip).

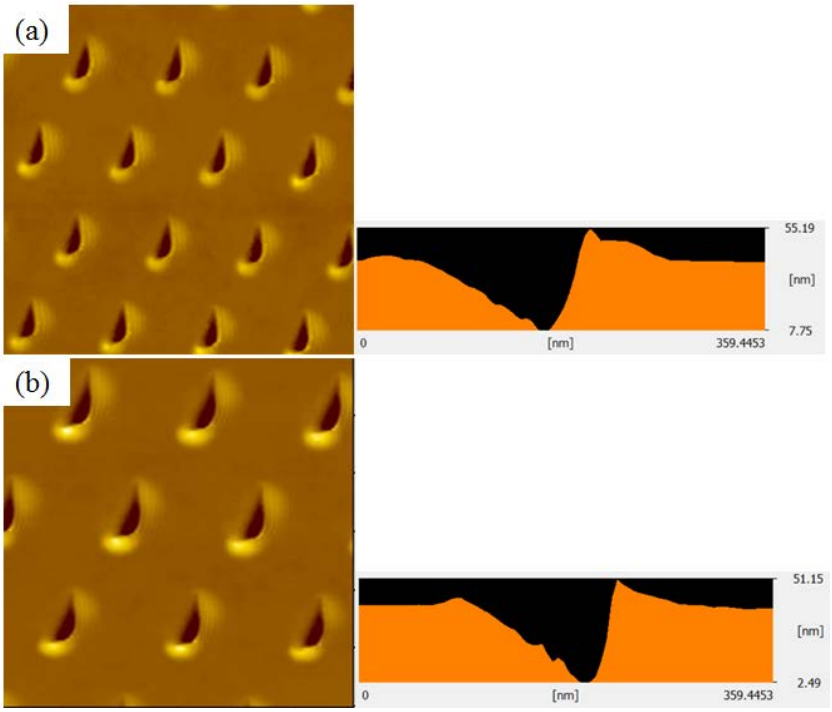

Figure 4.3 AFM image and cross sectional profile of indentation pattern measured by (a) new tip of same kind of using indentation experiments (NSG 30), and (b) high aspect ratio tip.

4.1 Changes in the shape and depth of the pattern according to the indentation speed

Figure 4.4 shows the appearance as seen from the side of AFM cantilever. When the AFM scanner is pushing up the AFM cantilever, the cantilever is subjected to a force from the lateral, y, direction as well as vertical, z, direction, as shown by red arrows in figure 4.4. This lateral force applies a torque to the tip, then rotational motion of the tip occurs based on the center of rotational motion, O, as shown in yellow arrow in figure 4.4. The rotational motion could create the change in the y direction, Δy, and eventually structure length is increased. We also could know that there may be a change in the z direction of structure depth, Δz, depending on the size of the rotational motion. We can describe this rotational motion as damped simple harmonic motion, which is the motion by spring constant of the AFM cantilever with the damping caused by the viscosity of the gold-PMMA system. So, we can easily express the rotation angle from a damped simple harmonic equation. In addition, we can expect that

$$\frac{d\theta^2}{dt^2} + 2\zeta\omega_0\frac{d\theta}{dt} + {\omega_0}^2\theta = 0 \quad (1)$$

where ω_0 is natural frequency of the system and ζ is a constant called the damping ratio. Here, the parameters of equation (1) are expressed as follows:

$$\omega_0 = \sqrt{\frac{k}{m}}$$

$$\varsigma = \frac{c}{2\sqrt{mk}}$$

where m is a mass, k is a spring constant, and c is a viscous damping coefficient of a system.

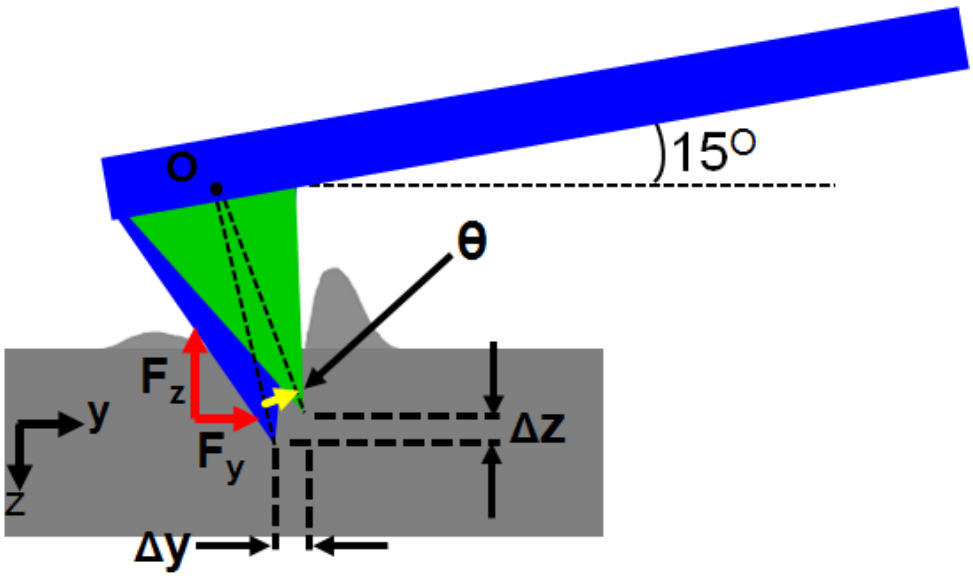

Figure 4.4 The picture of the side view on the cantilever in doing AFM indentation. When the AFM cantilever is pressing down the sample, the cantilever is subjected to a lateral and vertical force as indicated red arrows.

By the way, we can expect that the rotation angle, θ, would be very small because the length of AFM tip is about 10 μm and the structure depth is a few tens of nanometers. So, instead of the equation (1) about the angle, the expression can be written about the structural length. Therefore, the structure length, y, can be written as follows,

$$y(t) = y_1 + y_2 e^{-\tau/\tau_0} \quad (2)$$

where $y_1 > 0$ and $y_2 < 0$ are constants determined by boundary conditions, $\tau_0 = 1/\zeta\omega_0$ is the characteristic time of the system with viscous damping ratio, ζ, of the system and $\tau = d/v_i$ is the duration of time, which is the time a tip is moving to the indentation depth, d, with indentation speed v_i. The equation of the structure depth, z, also can be written the same way as equation (2). From this equation, as the duration of time increases, the structure length exponentially increases whereas the depth decreases exponentially. Figure 4.5 shows statistically analyzed depth and length of the structures as a function of time. The structure length increased as the duration of time increased, as shown by the blue dot in figure 4.5, while the depth decreased as the duration of time increased, as shown by the black dot in figure 4.5. Dashed lines show the fitting results for the data in figure 4.5. This plot is best described with equation (2). This result agrees with the model prediction that the length and depth of the structures exponentially depend on the indentation speed. These results indicate that rapid change begins between 10 ms and 50 ms. Furthermore, the critical speed is the speed determined by characteristic time. Using these results, we can explain the distortion of the structures' shapes in figure 4.2 (a), (b), and (c). When the duration of time is 10 ms, in the case of $\tau/\tau_0 < 1$, the tetrahedral shape of the AFM tip

makes a triangular indentation because there is little change in the structure length in the y direction, as shown in figure 4.2 (c). However, when the duration of time is 50 ms or 250 ms, in the case of $\tau/\tau_0 > 1$, the distorted half-circle shape became the triangular shape as shown in figure 2(a) and (b).

We can also compare this characteristic time with the value obtained by qualitative methods. If we assumed that the elastic constant of the system was determined by the PMMA because elastic modulus values of silicon and gold are more than 100 times that of the PMMA, we would find that the characteristic time is 10 ms with ζ = 2.27×10^{-2}, and ω_0 = 4.4 kHz (where $Q = f_0 / \Delta f$ = $4{,}400\,\text{Hz} / 200\,\text{Hz}$ = 22, so we can get $\zeta = 1/2Q =$ 2.27×10^{-2}), using the measured data in the literature[5]. We could easily know that the rapid change of the length and depth, based on this characteristic time, is the same as the previous description derived from the equation (2). These results indicate that the indentation speed must be faster than the critical speed determined by characteristic time.

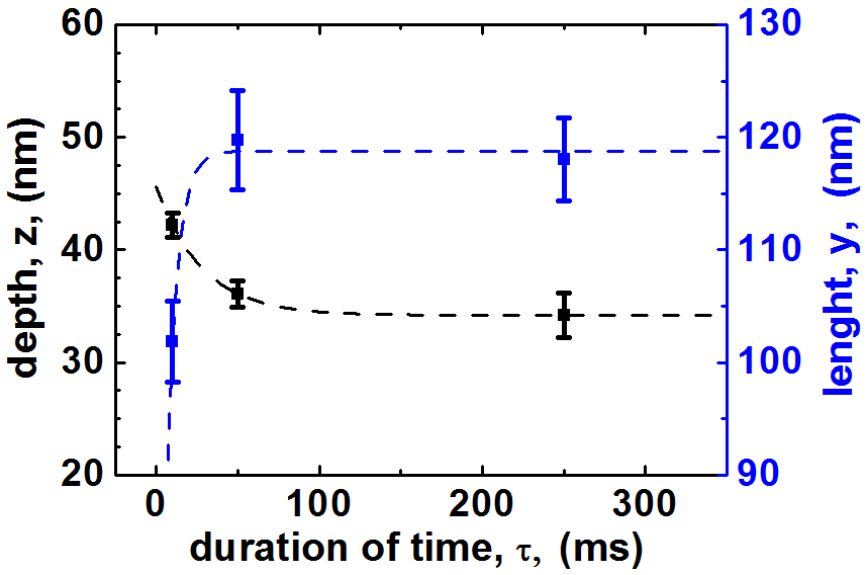

Figure 4.5 Depth and length of structure as a function of time. Dashed lines are the fitting results for the data using equation (2).

4.2 Changes in the substructure of the pattern according to the indentation speed

Figure 4.6 shows that the inverted 3-dimensional AFM image and cross sectional profile of dent hole pattern according to the change of indentation speed.

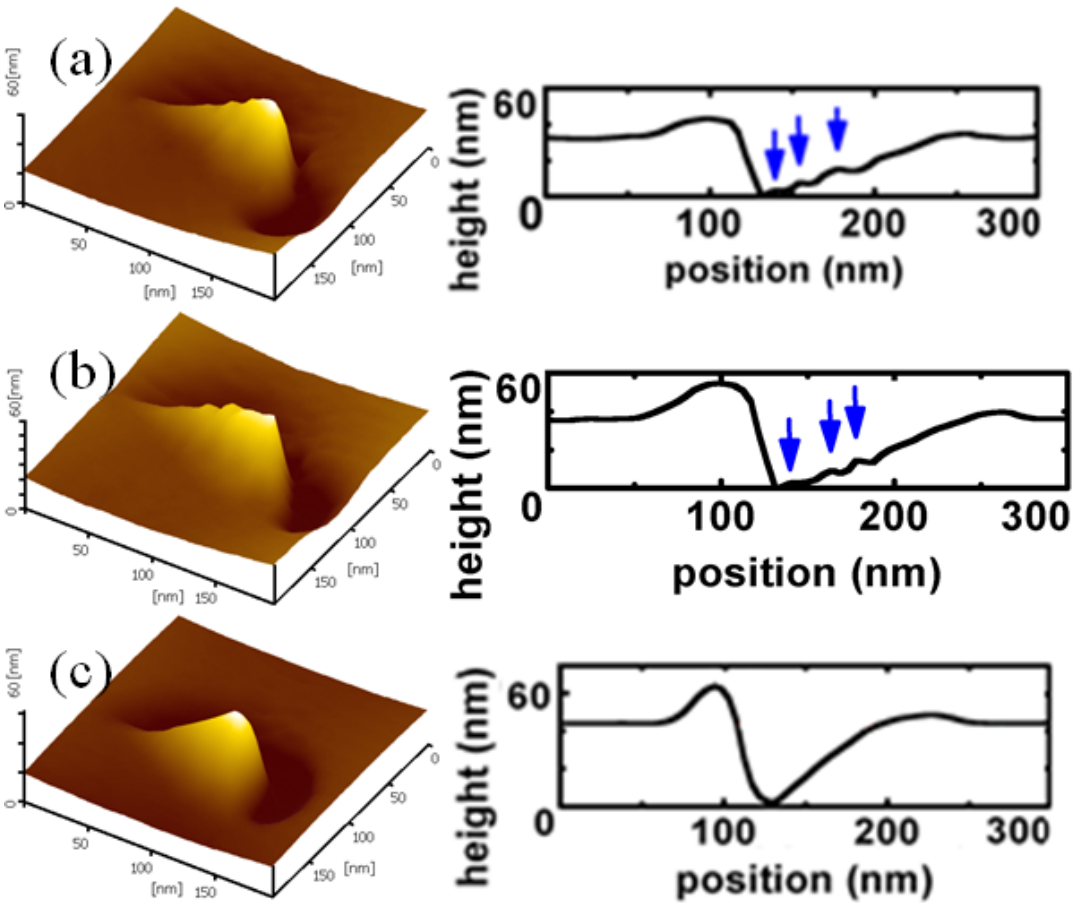

Figure 4.6 (a), (b), and (c) are the inverted 3-dimensional AFM image and cross sectional profile of dent hole pattern according to the change of indentation speed. Which is 0.2 μm/s, 1 μm/s, and 5 μm/s, respectively.

We could clearly see that there is the substructure in the inside pattern at the low speed of indentation as shown in figure 4.6 (a) and (b) (as marked with blue arrows in cross sectional profile), but couldn’t see at the high indentation speed as shown in figure 4.6 (c). We explained the observed speed dependence using the interaction of AFM tip and gold-PMMA structure which explains why and how the substructure was created.

Let's consider the system such as shown in figure 4.7. An elastic block on a substrate with weak spring (spring constant K_s). When we pull the block, if the speed, v_s, is greater than a critical speed, v_c, the motion of block continues without stopping. On the other hand, the speed is less than a critical speed, the block motion is different from those previously described. The moving block is stopped by frictional force. At this time, the elastic force of spring is proportional to the distance increases moved until the block stops, therefore the elastic force of spring become larger than the frictional force, and then the motion of the block starts again. The block is repeated this motion which is called stick-slip motion[1].

Now, let's explain the interaction between the AFM tip and the sample. There are two types of forces. The one is to hinder the motion of the tip, pinning force, and the other is to sustain that of the tip, shear force. If indentation speed is slower than critical speed, pinning force is larger than shear force; if indentation speed is faster than critical speed, then shear force is larger than pinning force. If the indentation speed is slower than the critical speed, the speed gradually decreases and eventually stops because the pinning force is larger than the shear force. At the same time, the elastic force of the cantilever grows proportional to the distance between the beginning point and the point where the tip stops moving.

Eventually, the elastic force will be larger than the damping force that resist against the movement of the tip, and then the motion of the tip starts again. This motion can be called stick-slip motion as previously described. We think that the substructures inside the indentation pattern were created by this stick-slip motion and rotational motion of AFM tip simultaneously acting on. However, if the indentation speed is faster than the critical speed, substructures will not be created because the tip moves without stick-slip. According to our experiments, the critical speed is considered as the value of between 5 μm/s and 1 μm/s of indentation speed. These results also indicate that the indentation speed must be faster than the critical speed in order to minimize additional motion of AFM tip which means minimizing the AFM tip damage.

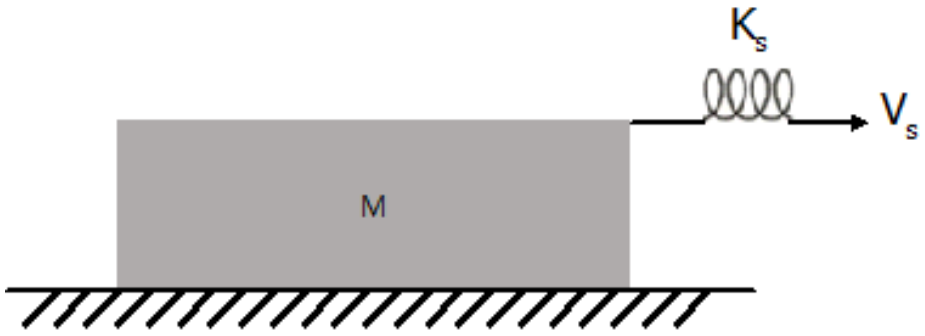

Figure 4.7 An elastic block on a substrate. If the spring constant K_s is very weak, the transition from steady to stick-slip motion will occur at the sliding velocity, V_c.

Bibliography

[1] B. N. J. Persson, in Sliding Friction, 2nd ed. Springer, Berlin, 2000 .

[2] Y.-J. Chen, J.-H. Hsu, and H.-N. Lin, Nanotechnology **16**, 1112 (2005)

[3] Ju-Hung Hsu, Chun-Yu Lin, and Heh-Nan Lina J. Vac. Sci. Technol. B **22** 2768 (2004)

[4] This FE-SEM pictures of the NSG30 and NSC05 are taken from the manufacturer's website as following. http://www.ntmdt-tips.com/products/view/nsg30, and http://www.ntmdt-tips.com/products/view/nsc05-10, respectively.

[5] T. Lee, R. S. Lakes, and A. Lal Rev. Sci. Instrum. **71** 2855 (2000)

Chapter 5

Conclusions

Using a noncontact consecutive-hole-indentation method by adjusting hole-hole distance that we developed, we made uniform, two-dimensional reproducible nanostructures, solving one of the problems associated with AFM indentation. Through the topographic and electrical measurements of the fabricated gold nanowires, we demonstrated that uniform and reproducible nanostructures can be fabricated with conventional silicon AFM tips without any special treatment such as diamond coating. This method minimized the tip damage by reducing the vertical and lateral forces acting on the tip when it presses on the substrate or moves between the thin gold layer-PMMA structures. Furthermore, the AFM indentation nanolithography method presented in this study is versatile. Although gold and PMMA were specifically used in this experiment, other combinations of metals and polymers can also be used.

We also investigated the relationship of the pattern structure and the indentation speed. The interactions between the tilted cantilever and the double-layer structure created the rotational motion follows the damped harmonic oscillator. The rotational motion predicts that the faster speed less elongation and deeper depth, which is consistent with our experimental results. As a result, the distortion of the structures is exponentially proportional to the time during which the tip is inserted into the sample. Furthermore, the interactions between the tip and the sample can create substructures

because of the stick-slip motion. These substructures and the distortion of the pattern occur when the indentation speed is slower than the critical speed. Therefore, AFM indentation should be performed by controlling the indentation speed. These results will help to further improve reproducibility and productivity.

Abstract in Korean

원자힘 현미경의 탐침 손상을 최소화 시키는 압입 식각 방법을 이용하여 재현성 있는 양자점과 나노선을 제작하였다. 균일한 양자점과 나노선은 2 층 구조에서 홀 패턴을 제작하고, 건식 식각 공정을 통해 폴리머를 제거한 후, 이 압입 홀 패턴을 통해 금속 증착을 실행하는 공정을 통해 제작되었다. 2 층 구조는 실리콘 기판 위에 폴리머 (PMMA)를 스핀 코팅 한 후 얇은 금 박막을 올려서 제작하였다. 탐침 압입 시에 2 층 구조에 가하는 힘은 탐침이 얇은 금속 박막을 통과하되 실리콘 기판에 닿지 않도록 조정하여 탐침의 손상을 최소화하였다. 이 2 층 구조에서의 금 박막은 건식 식각과정에 금속 마스크로 사용된다. 압입 홀을 통해 폴리머는 등방성 식각 되어, 금 박막과 기판 사이에는 언더컷 구조가 생성된다. 이 언더컷 구조는 폴리머 잔여물이 없는 상태에서 기판 위에 금속 증착이 가능하게 해준다. 이러한 압입 홀 패턴을 통해 실리콘 기판 위에 금을 증착 함으로써 양자점을 연속적으로 제작하였다.

2 층 구조에서 홀 간의 거리를 조절한 연속적인 홀 압입 방법을 이용해 금 나노선을 제작하였다. 균일한 형상과 전기적으로 매우 우수한 성질을 가진 금 나노선을 반복적으로 제작할 수 있었다. 이 결과는 우리가 나노선을 제작한 방법이 우수함을 보여준다. 또한 전자현미경을 이용해 탐침을 직접 비교함으로써 우리가 개발한 홀 간의 거리를 조절한 연속적인 홀 압입 방법이 기존에 알려진 일반적인 식각방법보다 탐침 손상이 적다는 것을 확인 할 수 있었다. 또한 금속을 포함한 벌지를 초음파를 이용해 제거하는 방법도 연구하였다.

원자힘 현미경의 탐침은 약간 기울어져 장착되어 있는데, 이러한 구조는 탐침의 압입 속도에 따른 패턴의 형상 변화를 만들어 낸다. 금 박막과 폴리머로 이루어진 2 층 구조에서 탐침의 압입 속도가 느릴 때는 왜곡된 반원 모양의 패턴 형상이 생겨났다. 반면에 압입 속도가 빠를 때는 이러한 왜곡이 없는 삼각형 형태를 가진 탐침 모양의 패턴이 생겨났다. 또한 압입 속도가 증가할수록 패턴의 깊이는 증가했고, 반면에 패턴의 길이는 감소했다. 우리는 이러한 패턴 형상의 변화가 원자힘 현미경의 탐침이 2 층 구조 안에서 회전 운동을 함으로써 생겨난 것을 알아냈다.

주요어: 원자힘 현미경 (AFM), 2층 구조, 연속적인 홀 압입 방법, 압입 식각, 폴리머 (PMMA), 양자점, 나노선, 압입 속도

학번: 2002-30936

Acknowledgement